(2)

Final Report

OPTICAL COMPUTING BASED ON THE HOPFIELD MODEL FOR NEURAL NETWORKS

CALIFORNIA INSTITUTE OF TECHNOLOGY

PASADENA, CALIFORNIA

(2)

Contract/Grant N00014-85-K-2035

Final Report

OPTICAL COMPUTING BASED ON THE HOPFIELD MODEL FOR NEURAL NETWORKS

Demetri Psaltis, Ken-Yuh Hsu, Hsin-Yu Li

Department of Electrical Engineering
California Institute of Technology
Pasadena, California 91125

DEPARTMENT OF THE NAVY
OFFICE OF NAVAL RESEARCH
RESIDENT REPRESENTATIVE

565 S. Wilson Avenue
Pasadena, California 91106-3212

1 Introduction

Associative memories are one of the most interesting applications of neural networks. In general, an associative memory stores a set of information, called memories. The information is stored in a format such that when an external stimulus is presented into the system, the system evolves to a stable state that is closest to the input data. We can view this process as a content-addressable memory since the stored memory is retrieved by the contents of the input and not by the specific address. In other words, the memory can recognize distorted inputs as long as the input provides sufficient information. Later in this report we will show the characteristics of the associative memory by presenting distorted versions of the stored images, e.g., rotated, scaled, shifted ones, etc. to the system and see how it converges.

In this report we present holographic implementations of Hopfield's model of neural network [1, 2]. This model has a very simple structure and is easy to implement. However, its principles and characteristics, e.g., neuron thresholding, global interconnections between the neurons, and feedback dynamics, are very flexible hence the results can be easily extended to other types of neural networks. In the following section, the basic principle of the Hopfield network and its one-dimensional implementation are reviewed. The optical implementation of the network for processing two-dimensional informations is presented in Section 3 and its experimental results are presented in Section 4. Special attention is focused on the dynamical phenomena of the feedback loop. Section 5 discusses the trade-off between distortion tolerance and image-recognition capability of the associative memory. Mathematical modeling of this particular optical loop and its convergence proof are presented in Section 6.

2 The Hopfield Model of Associative Memory

The basic structure of the Hopfield type neural network for two-dimensional (2-D) informations is shown in Fig. 1. It is a single-layer network with feedback. As shown in the figure there are two ingredients in the network: the neurons and the interconnection tensor. The neurons are distributed in a plane called the neural plane. The neurons receive input images, perform nonlinear thresholding on the received input, and then re-emit output patterns. The output of each neuron is connected to the input of every other neurons to form a feedback network.

There are several ways to implement a 2-D neural plane [3]. Optoelectronic techniques integrate photo-detectors, electronic amplifiers, and light emitting sources to form a neural plane [4]. The thresholding characteristics of the neurons are controlled by adjusting the gains of the electronic amplifiers. Photorefractive $BaTiO_3$ crystals operating in a saturable, two-beam amplification mode provides another alternative [5] where the modulation depth between the two beams is an adjustable parameter. In our experiments we use the combination of an image intensifier and a liquid-crystal light valve (LCLV) to simulate the neural plane. For the case of 2-D neurons the interconnection pattern is a four-dimensional tensor. In our experiments the interconnection tensor is implemented by two Fourier-transform holograms. The holographic techniques of making this interconnection will be presented in the next section.

There are two phases involved in operating the Hopfield network, the learning phase

A-1

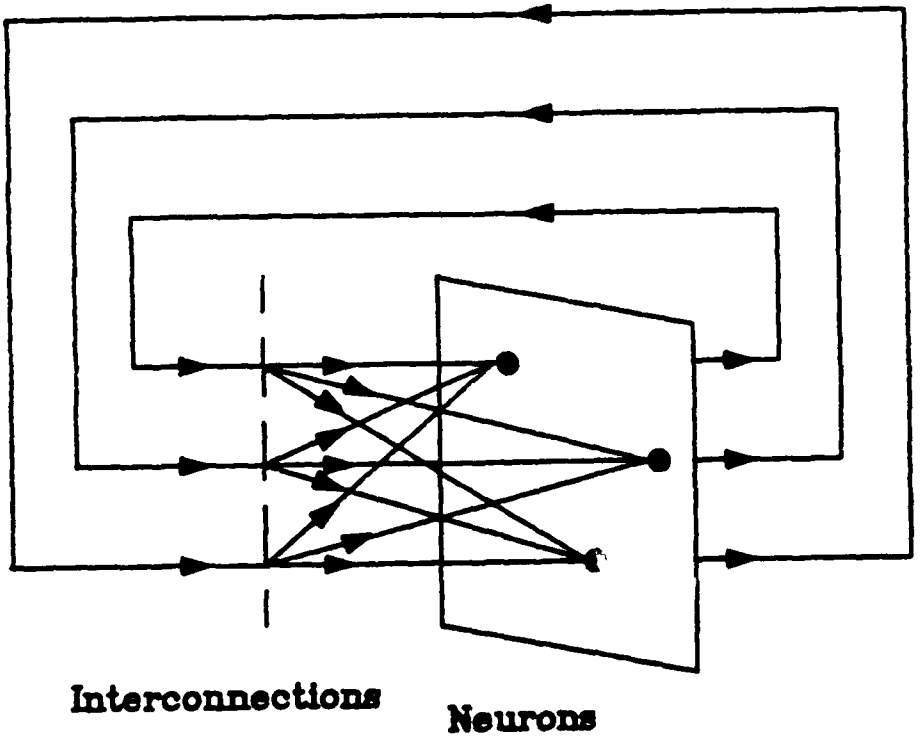

Fig. 1: The 2-D Hopfield-type Neural Network.

and the recalling phase. In the learning phase, the information to be stored is recorded using an outer product scheme. This storage specifies the interconnection strengths between the neurons. In the recalling phase, an external input is presented to the system. The state of the system then evolves according to the correlation between the input and the stored data. Consider the learning phase in the 1-D case; we first store M N-bit binary words in a matrix $\omega_{i,j}$ according to

$$\omega_{i,j} = \begin{cases} \sum_{m=1}^{M} v_i^m v_j^m, & \text{if } i \neq j; \\ 0, & \text{otherwise,} \end{cases} \tag{1}$$

where $v_i^m = \pm 1$, $i = 1, \cdots, N$, is the ith bit of the mth memory. This matrix can be calculated and recorded in a program for simulations or it can be plotted on a transparency for optical experiments. The recording of this synaptic matrix completes the learning phase. In the recalling phase, external data are fed into the system and iterations are induced. For example, suppose $\mathbf{v}^{m0}$, the mth stored vector, is presented into the system. This vector is then multiplied by the stored matrix $\omega_{i,j}$, giving the output of the first iteration:

$$\begin{aligned} \hat{v}_i^{m0} &= sgn\left\{\sum_{j=1}^{N} \omega_{i,j} v_j^{m0}\right\} \\ &= sgn\left\{\sum_{j=1}^{N}\left[\sum_{m=1}^{M} v_i^m v_j^m\right] v_j^{m0}\right\} \qquad (2) \\ &= sgn\left\{(N-1)v_i^{m0} + \sum_{m\neq m0}^{M}\left[\sum_{j=1}^{N} v_j^m v_j^{m0}\right] v_i^m\right\}, \qquad (3) \end{aligned}$$

where $sgn\{\cdot\}$ means the thresholding function,

$$sgn\{f(x)\} = \begin{cases} 1, & \text{if } f(x) \geq 0; \\ -1, & \text{if } f(x) < 0. \end{cases} \tag{4}$$

The thresholded result of the first iteration re-enters the system for the next iteration so that the system evolves continuously. We see that in Eq. 3 two terms result from each iteration: The first term resembles the mth memory which we call the signal; the second is the crosstalk between the mth vector and other vectors, which we call the noise. We assume that the binary words are chosen randomly so that each bit is statistically independent; i.e., $P[v_i^m = 1] = P[v_i^m = -1] = 1/2$; then the signal-to-noise ratio (SNR) before thresholding is

$$\begin{aligned} SNR &= \frac{E[\hat{v}_i^{m0}]}{\sqrt{var[\hat{v}_i^{m0}]}} \\ &= \sqrt{(N-1)/(M-1)} \\ &\approx \sqrt{\frac{N}{M}}. \end{aligned} \tag{5}$$

If N is sufficiently larger than M, then with high probability each element of $\hat{v}_i^{m0}$ equals that of v_i^{m0}. Therefore, the stored vector $\mathbf{v}^{m0}$ remains a stable state of the system in iterating operations. It was shown in [6,7] that if the stored vectors are to be stable states, then the number of memories that can be stored in the system is limited by $M < N/(4 \ln N)$.

From Eq. 2 we see that we need three steps to implement the Hopfield network: vector-matrix multiplication, thresholding, and feedback. This was first done by Psaltis and Farhat using optoelectronic techniques [8,9]. They used a computer-generated transparency to provide the interconnection matrix. A 1-D array of 32 photodiodes followed by electronic thresholding plus a 1-D array of 32 LEDs was used to simulate 32 neurons. The arrays were used to detect and emit 32-bit data vectors. An optical vector-matrix multiplier was used to perform the multiplication between the the data vector and the transparency matrix. The multiplied result was detected by the photodiode array. The detected signal of each photodiode was electronically thresholded and fed back to the corresponding LED for further iterations. This system successfully demonstrated the dynamics and the capability of associative information recall of feedback neural networks. Another architecture using acousto-optics also demonstrated similar functions [10]. In this report we are interested in the processing of 2-dimensional images. The design and its optical implementation are presented in the following section.

3 Optical Implementation of the Associative Memory Loop

In this section we consider the implementation of the Hopfield-type neural network for 2-dimensional images. The interconnection pattern for 2-D images is described by the following equation:

$$\omega(x, y; \xi, \eta) = \sum_{m=1}^{M} f_m(x, y) f_m(\xi, \eta), \tag{6}$$

where $f_m(x, y)$ is the mth image to be stored, and M is the total number of images to be stored. Note that $\omega(x, y; \xi, \eta)$ is a four-dimensional tensor. It cannot be implemented straightforward using a single transparency since a 2-D optical system has only two spatial coordinates. One could obtain additional variables by using wavelength multiplexing and time-domain processing. In [8], Psaltis and Farhat proposed a spatial-frequency multiplexing method in which a 2-D array of 2-D holograms, each separated by different spatial-frequencies, was used to perform the 4-D interconnection. Jang, et al. used a 2-D array of $N \times N$ diffused holograms to obtain the 4-D interconnection [11, 12].

In this report we approach this problem from another point of view. Recall that in the recalling phase, the output of the system is described by the iterating equation

$$\hat{f}(x, y, t+1) = g\left\{ \int\int \omega(x, y; \xi, \eta) f(\xi, \eta, t) d\xi d\eta \right\}, \tag{7}$$

where $g\{\cdot\}$ represents the nonlinear thresholding of the neurons, $f(x, y, t)$ is the input to the system at time t, and $\hat{f}(x, y, t+1)$ is the output of the system. By inserting the expression of $\omega(x, y; \xi, \eta)$ into this equation and rearranging the order of integration and

summation, we obtain

$$\hat{f}(x,y,t+1) = g\left\{\iint\left[\sum_{m=1}^{M} f_m(x,y)f_m(\xi,\eta)\right] f(\xi,\eta,t)d\xi d\eta\right\}$$
$$= g\left\{\sum_{m=1}^{M} f_m(x,y)\left[\iint f_m(\xi,\eta)f(\xi,\eta,t)d\xi d\eta\right]\right\}$$
$$= g\left\{\sum_{m=1}^{M} f_m(x,y)\left[\iint f_m(\xi,\eta)f(\xi-x,\eta-y,t)d\xi d\eta\right]_{x=0,y=0}\right\}. \qquad (8)$$

From Eq. 8 we can see that the implementation of the 2-D associative memory can be achieved in three steps [13]. The first step is to perform the inner product of the input image f with each of the memories f_m. Second, each inner product is multiplied by the associated memory. Third, these products are summed over all memories and thresholded by the neurons for iterations. The implementation of these steps matches holographic techniques exactly. The idea is shown in the block diagram of Figure 2.

The first step described above can be realized by sampling the correlation pattern at the origin in Vander Lugt system [14]. The first correlator and the pinholes carry out this operation. The signal passing through the pinholes reconstructs the images from the second correlator. This carries out the second step. In the final step, the reconstructed images are summed up at the input side of the neurons, in this case the writing side of the LCLV. The LCLV is used to simulate a plane of neurons to perform the thresholding and provides a signal for further iterations.

The operation of the associative loop can be explained with the aid of the diagram shown in Fig. 3. In this example four images are spatially separated and stored in the Fourier-transform holograms H_1 and H_2 as shown in the figure. When the input pattern **A** is presented on the plane P_1 of the system, the first correlator produces the auto-correlation pattern along with three cross-correlations on plane P_2. The pinhole array on P_2 samples these correlation patterns at the center of each pattern where the inner products between the input and each of the stored images form. Each of the four beams that pass through the pinholes act as delta functions, reconstructing from the second correlator the four images stored in hologram H_2. These reconstructed images are spatially translated according to the position of each pinhole and superimposed on plane P_1. At the center of the output plane of the second correlator we obtain the superposition of the four stored images. The stored image that is most similar to the input pattern gives the strongest correlation signal, hence the brightest reconstructed image. Here in Fig. 3 we show only the bright image that is reconstructed by the strongest auto-correlation peak. The weak read-out signal that is due to cross-correlations can be eliminated somehow by thresholding by the LCLV. The output of the LCLV becomes the new input image for the loop and forms a closed loop. The stable pattern that forms as a recirculating image in the loop is the stored image that is most similar to the original input. This image stays locked in the loop even when the external input in turned off.

In the system that we described in the previous paragraph, the images are recorded in a conventional Fourier-transform hologram, as shown in Fig. 4. The four images, **A**,

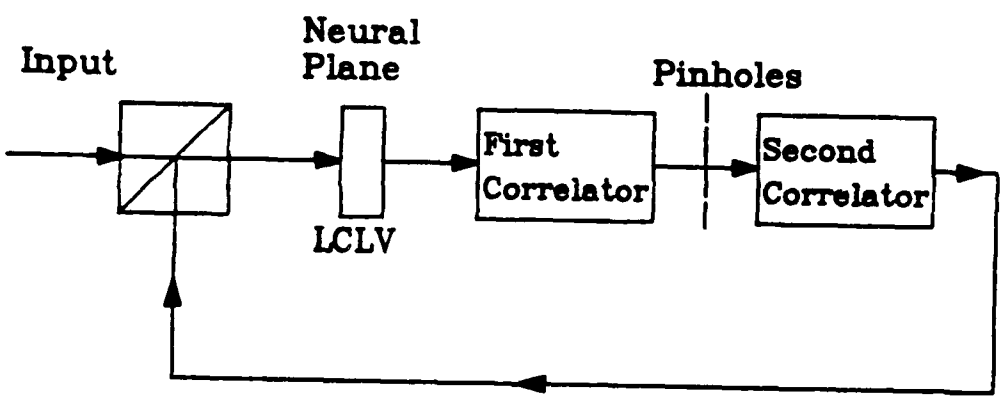

Fig. 2: Block Diagram of the Optical Loop.

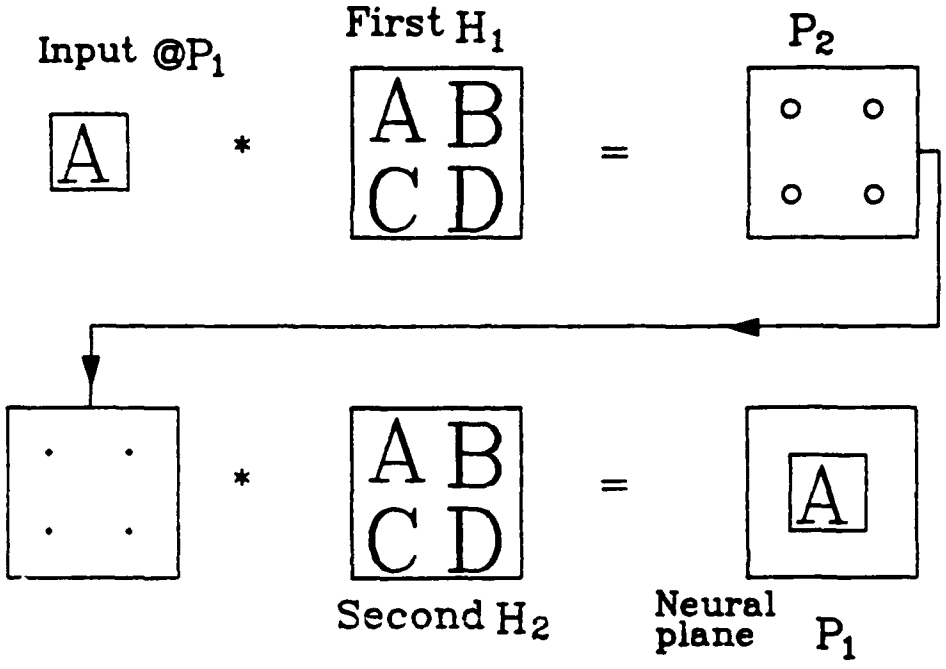

Fig. 3: Operational Principle of the Optical Loop.

B, C, D, in this example are spatially separated at the input plane. A single plane wave is used as the reference. We record two identical holograms, H_1 and H_2, then put one in each of the two correlators of Fig. 2. A pinhole array with pinhole separations equal to that of the corresponding original images is placed at the correlation plane to sample the correlation signal.

The schematic diagram of the architecture of the above design is shown in Fig. 5; and a photograph of the experimental apparatus is shown in Fig. 6. In the system shown in Fig. 5, the LCLV at plane P_1, the beam splitter cube BS_1, the lenses L_1, L_2, and the hologram H_1 form the first correlator. The part consisting of P_2, L_3, H_2, L_4, BS_3, and P_1 form the second correlator. The input pattern is imaged onto the LCLV by lens L_i and through beam splitter BS_3. A collimated argon laser beam illuminates the read-out side of the LCLV through beam splitters BS_2 and BS_1. A portion of the reflected light from the LCLV that propagates straight through BS_1, is diverted by BS_2, and it is imaged by lens L_0 onto a CCD television camera. This provides real time monitoring of the activity of the system. The portion of light that is reflected by BS_1 into the loop is Fourier-transformed by lens L_1 and illuminates hologram H_1. The correlation between the input image and each of the stored images is projected on plane P_2. The pinhole array at P_2 has spacing corresponding to the spatial separations of the stored images. The remainder of the optical system from P_2 back to the neural plane P_1 is essentially a replica of the first half, with the hologram H_2 storing the same set of images at H_1.

We now describe the operation of this system analytically. The amplitude transmittance of the transparency from which the holograms are recorded is

$$f(x,y) = \sum_{m=1}^{M} f_m(x - a_m, y - b_m), \tag{9}$$

where $f_m(x,y)$ is the amplitude transmittance of the mth image at the input plane in Fig. 5, (a_m, b_m) is the center of $f_m(x,y)$ on the (x,y) plane, and M is the total number of recorded images. In our experiments, the separations between different images are the same, i.e., $a_m = b_m = ma$, where a is a constant. The M images in Eq. 9 are Fourier-transformed to interfere with a reference wave $e^{-j2\pi ub}$ and recorded on a holographic plate. The amplitude transmittance of the developed hologram is

$$\begin{aligned} T(u,v) &= \left| \sum_{m}^{M} F_m(u,v) e^{-j2\pi(ua_m + vb_m)} + e^{-j2\pi ub} \right|^2 \\ &= \sum_{m}^{M} F_m^*(u,v) e^{j2\pi[u(a_m - b) + vb_m]} + \text{Complex Conjugate} + \text{DC terms}, \end{aligned} \tag{10}$$

where (u,v) is the coordinate in the Fourier plane. This hologram is placed in planes H_1 and H_2 of the system. In the above equation we are interested only in the first term since it is the part which the input image will correlate with. Suppose the amplitude of the input image at time t is $f(x,y,t)$ at plane P_1, then after hologram H_1 the light amplitude

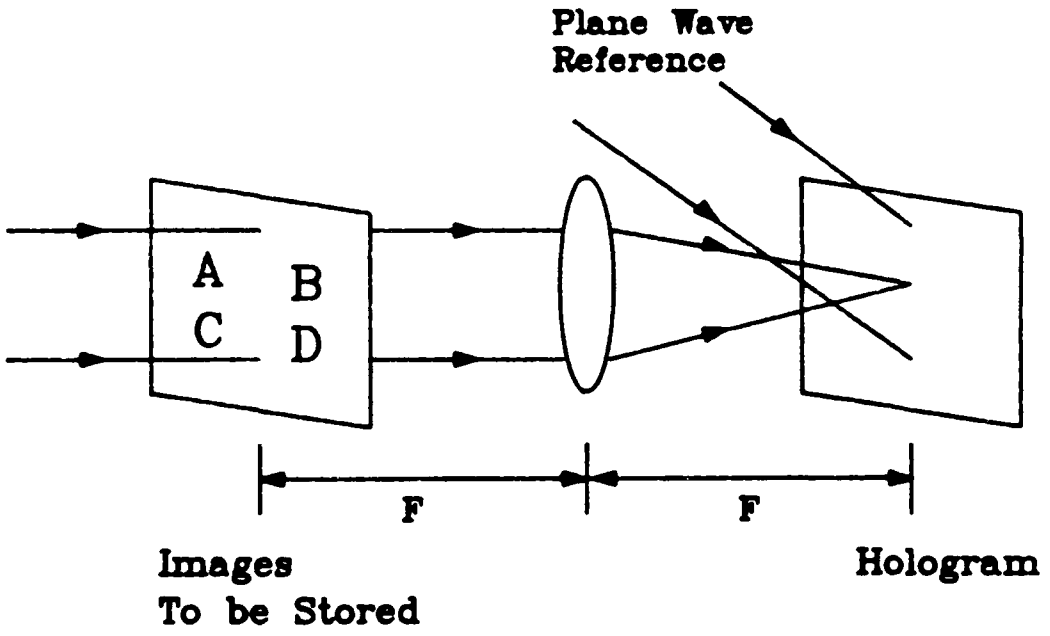

Fig. 4: Recording of the Fourier Transform Hologram.

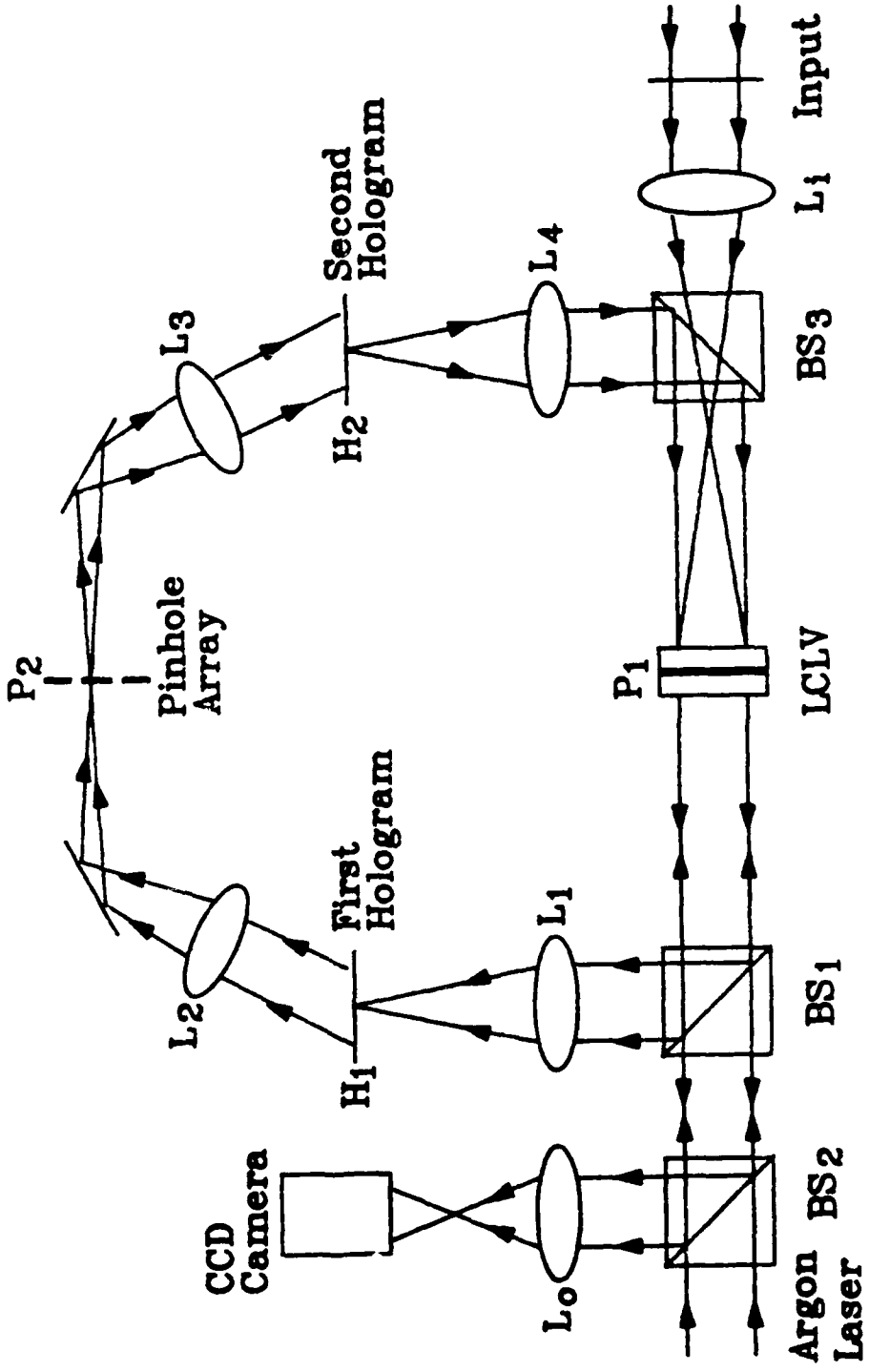

Fig. 5: Schematic Diagram of the Optical Loop.

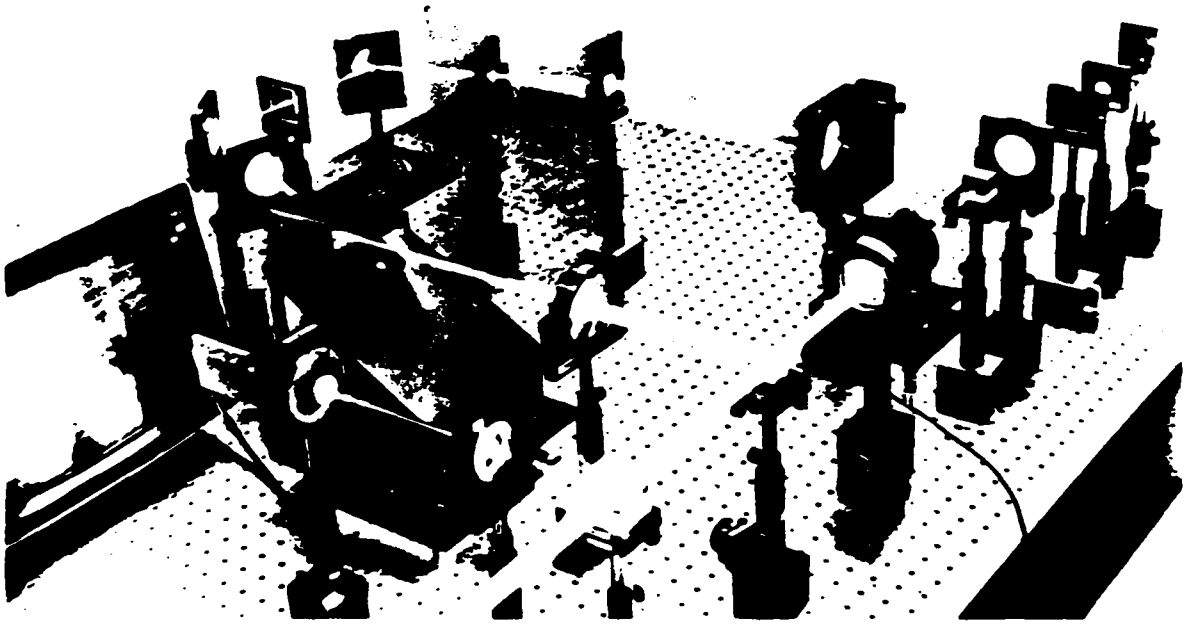

Fig. 6: Photograph of the Optical Loop.

diffracted by the first term is

$$\sum_{m=1}^{M} F(u,v,t)F_m^*(u,v)e^{j2\pi[u(a_m-b)+vb_m]}. \tag{11}$$

At the correlation plane, P_2, the light amplitude is the Fourier transform of the above term:

$$\begin{aligned}&\sum_{m=1}^{M} f(-x',-y',t) \star f_m(-x',-y') * \delta(x'-(a_m-b),y'-b_m)\\ &\equiv \sum_{m}^{M} h_m(-x',-y',t) * \delta(x'-(a_m-b),y'-b_m),\end{aligned} \tag{12}$$

where $h_m(-x',-y',t)$ represents the correlation between f and the memory f_m, $\star$ means correlation and $*$ means convolution, and $(x\prime,y\prime)$ is the coordinate in correlation plane. The above equation is sampled by the array of pinholes having diameter W and locating at the positions (a_m-b,b_m). In the limit $W \to 0$, the pinholes can be described as delta functions. Thus, the signal passing through the pinholes becomes

$$\begin{aligned}&\sum_{m=1}^{M}\left[h_m(-x',-y',t) * \delta(x'-(a_m-b),y'-b_m)\right] rect\left(\frac{x'-(a_m-b)}{W}\right) rect\left(\frac{y'-b_m}{W}\right)\\ &\approx \sum_{m=1}^{M} h_m(0,0,t)\delta(x'-(a_m-b),y'-b_m), \quad as\ W \to 0.\end{aligned} \tag{13}$$

This signal reconstructs images from the hologram H_2, giving

$$\begin{aligned}&\sum_{m=1}^{M}\sum_{m'=1}^{M} h_m(0,0,t)e^{-j2\pi[u(a_m-b)+vb_m]}F_{m'}^*(u,v)e^{i2\pi[u(a_{m'}-b)+vb_{m'}]}\\ &= \sum_{m=1}^{M}\sum_{m'=1}^{M} h_m(0,0,t)F_{m'}^*(u,v)e^{-j2\pi[u(a_m-a_{m'})+v(b_m-b_{m'})]}.\end{aligned} \tag{14}$$

This signal is Fourier-transformed back to the input side of the neural plane P_1. The total field amplitude is

$$\hat{f}(x,y,t) = \sum_{m=1}^{M}\sum_{m\prime=1}^{M} h_m(0,0,t)f_{m\prime}^*(x+(a_m-a_{m\prime}),y+(b_m-b_{m\prime})). \tag{15}$$

There are $M \times M$ images reconstructed and imaged on the neural plane. Only the terms with $m = m'$ are on-axis and aligned with the original input $f(x,y,t)$. If we put a window

centered at the optical axis, with the size equal to the size of each memory, we observe only the terms where $m = m'$:

$$\hat{f}(x,y,t) = \sum_{m=1}^{M} h_m(0,0,t) f_m^*(x,y). \tag{16}$$

The intensity of this light amplitude is detected by the photoconductor of the LCLV and gives an output light amplitude, to the first order, proportional to the detected intensity. Thus, the images are fed back into the loop. The images reconstructed by the auto-correlation peak become stronger and stronger until the LCLV saturates, whereas the images reconstructed by the cross-correlations become weaker and weaker until they die out.

The key elements in this optical loop are the holograms, the pinhole array, and the threshold device. The holograms in this system are thermoplastic plates. They have a resolution of 800 lines per millimeter over an area of one square inch. If we put a mirror [13] or a phase conjugate mirror [15, 16, 17] at the pinhole plane P_2 to reflect the correlation signal back through the system, then we only need one hologram to form the associative memory. But then it losses feedback dynamics. The use of two holograms, however, not only provides dynamics but also improves system performance. We make the hologram at H_1 with a high-pass characteristic so that the input section of the loop has high spectral discrimination. On the other hand, we want the feedback images to have high fidelity with respect to the original images. Thus, the hologram at plane H_2 must have broad-band characteristics. We use a diffuser to achieve this when making H_2. Fig. 7(a) shows the four original images. Fig. 7(b) shows the images reconstructed from the first hologram H_1, and Fig. 7(c) shows the images reconstructed from the second hologram H_2. As expected, Fig. 7(b) is a high-pass version of the original image while Fig. 7(c) is broad band.

The pinhole array at plane P_2 samples the correlation signal between the image coming from the LCLV and the images stored in hologram H_1. The pinhole diameter used in these experiments range from 45 μm to 700 μm, depending on the images to be stored and the desired system performance. If the pinhole size is too small, then the light that passes through it to reconstruct the feedback image is too weak to be detected by the LCLV and no iterations can occur. On the other hand, large pinholes introduce excessive blurring and cross-talk in the feedback and make the reconstructed images unrecognizable. The pinhole size also affects the shift invariance property of the loop. In order to be recognized, the auto-correlation peak from an external image should stay within the pinhole. Larger pinholes allow more shift in the input image. The system performance under different selections of pinhole diameters will be discussed in the next section.

The purpose of the threshold device in this system is three-fold. The first is to bring into the system a coherent image from the external input (although either coherent or incoherent images can be used as the input). The second is to provide a thresholding operation to the feedback signal so that cross-correlation is reduced in successive iterations. The third is to provide gain to the feedback signal. The optical signal is attenuated in the loop because of the diffraction efficiencies of the Fourier transform holograms and the losses from pinholes as well as lenses and beam splitters. Therefore, we need to have optical gain to compensate this loss. In our system this is achieved by adding an image intensifier at the

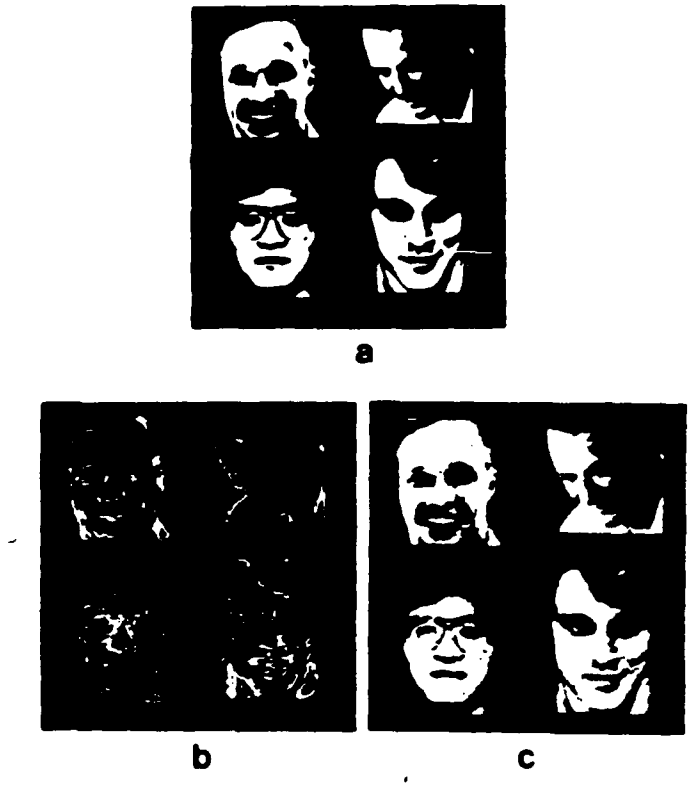

Fig. 7: Images Stored in the Holograms. (a) The original images. (b) Images reconstructed from H_1. (c) Images reconstructed from H_2.

photoconductor side of the LCLV. As described in Chapter 2, the microchannel plate of the image intensifier is sensitive to a minimum incident intensity of approximately 1 nW/cm^2 and reproduces the input with an intensity 10^4 times brighter (10 $\mu W/cm^2$). This is bright enough to drive the LCLV. If we use a beam with intensity equal to 10 mW/cm^2 to read the LCLV, then the intensity of the output light is approximately 1 mW/cm^2. Thus, the combination of the image intensifier and the LCLV provides optical gain up to 10^6. This optical gain is similar to a sigmoid function and its slope can be adjusted by changing the bias voltage of the image intensifier. In Section 5 we will see that the setting of the gain is the key parameter that mediates the trade-off between distorsion invariance and the discrimination capability of the loop.

4 Experimental Results

In this section we show, experimentally, many interesting properties of the optical associative loop. These include retrieval of complete images from partial inputs, recognition of the shifted, rotated and scaled images, error-correction capability, and neural network dynamics. The most interesting among these is the system dynamics. This is a unique property of a neural network with feedback and threshold. The state of the system evolves in time and the dynamics are determined by the operation parameters . The dynamics provide a trade-off for optimal system design. The dynamics of the associative memory is presented in the following section and the trade-off issue will be discussed in Section 5.

4.1 The Dynamics of the Associative Loop

According to the characteristics of the optical components, i.e., active or passive, the optical associative loop of Fig. 5 can be lumped into a simplified diagram as shown in Fig. 8(a). Since the LCLV provides optical gain and thresholding to the signal, it is represented as the component **Gain** in Fig. 8(a). The other parts of the loop are all lossy components and are represented as the component **Loss** in Fig. 8(a). This includes the beam-splitter cubes, the lenses, the mirrors, the pinhole array, and the holograms. The circulation of the optical signal in the loop is also shown by the arrows in the figure. Note that in the loop the output of the neurons forms the input to the lossy part, and the output of the lossy part becomes the new input for the neurons in the next iteration.

Let us consider the loop dynamics. The dynamics of the recall process can be described by using an iteration map formed by the gain and loss curves as shown in Fig. 8(b). In the figure the sigmoid curve represents the input-output response of the neurons. The slope of the curve is proportional to gain of the neurons, whereas the slope of the straight line is proportional to loop loss because of the holograms and pinholes and is drawn on the same diagram as the input-output response of the neurons. The intersection point of this line with the neural gain curve at Q_1 determines the loop threshold level, and the intersection point Q_2 represents a stable point. If the initial condition of the neuron is above the threshold level θ_1, such as I_1 shown in the figure, the signal grows after each iteration until it arrives and latches at Q_2. On the other hand, if the initial condition is below θ_1, such as I_2 shown in the figure, the signal will decay to zero. The number of iterations depends on the distance of the initial condition from the threshold.

The loop dynamics was measured by controlling two shutters as shown in Fig. 8a. The temporal response of the loop to an input pattern is shown in Fig. 9. The lower trace

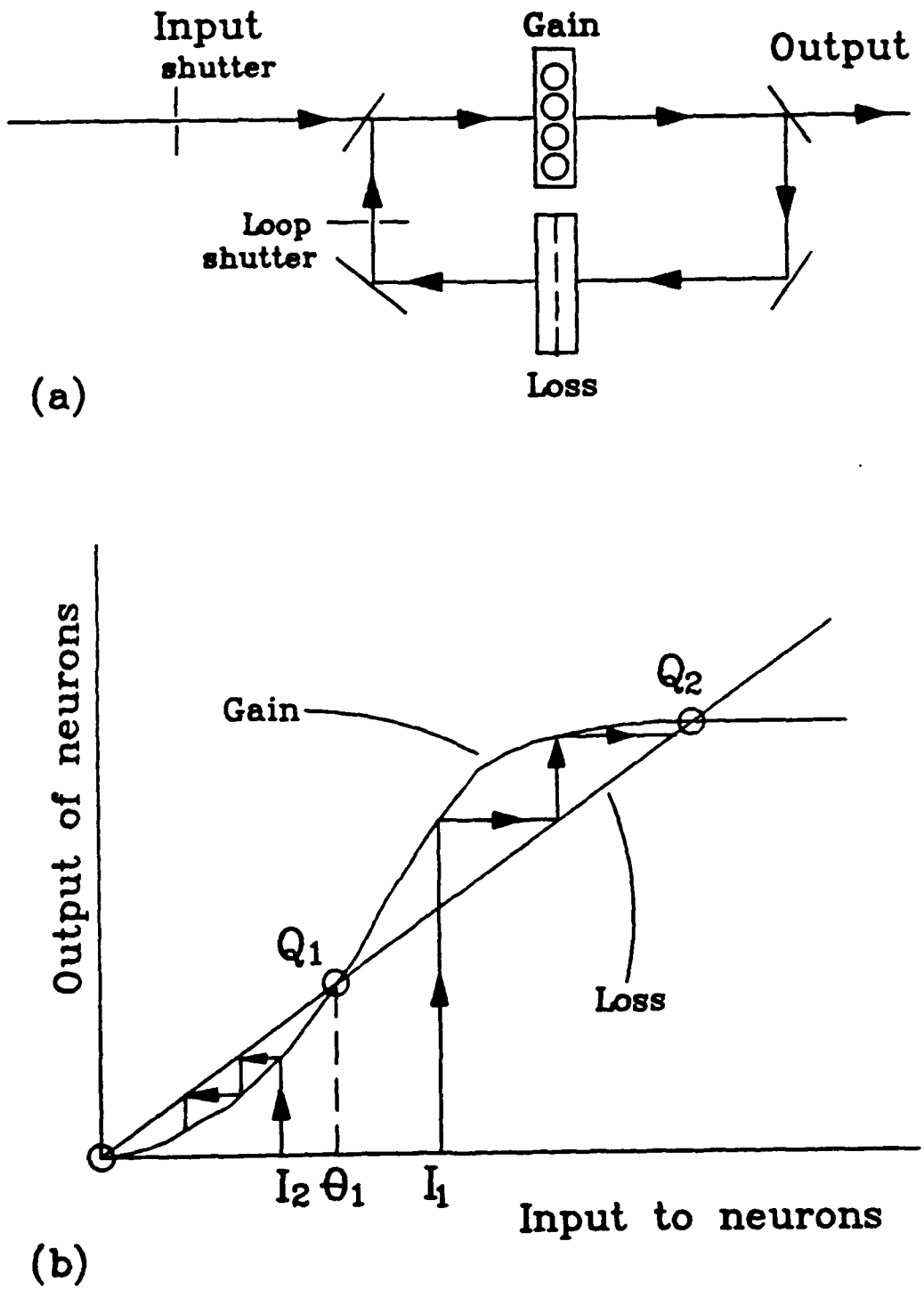

Fig. 8: Iterations in the Optical Loop. (a) The gain and loss components in the loop. (b) The iterations in the loop.

represents the intensity of the external input image and the upper trace represents the corresponding light intensity detected at the loop output. Before time t_1, both shutters are **OFF** and the responses are low. At time t_1 the input shutter is turned **ON**; hence the lower trace becomes high, but the loop shutter remains **OFF**. The upper trace shows the corresponding response of the neurons to the external input. The rise time of the LCLV is approximately one second in this experiment. At time t_2 the loop shutter is turned **ON** and the loop is closed. The feedback signal arrives at the neurons as an additional input and iteration occurs. From Fig. 9(a) we see that it takes about two seconds for the loop to reach a stable state. At time t_3 the input shutter is turned **OFF**; hence the lower trace becomes low. However, the loop remains latched to a stable state, which is one of the stored images. Fig. 9(b) shows the same experiment but with input intensity reduced to one-third of the first input. The first rise of the upper trace shows that the rise time of the neurons remains one second. And the second rise of the upper trace shows that it takes approximately four seconds for the loop to reach its stable state. However, after the input is turned off, the loop gives the same output intensity. This example shows that initial conditions affect the dynamics of the loop but do not affect the final state of the system. Fig. 10 shows the iteration map of this experiment where the initial input I_2 is lower than I_1. It shows that I_2 takes more iterations to reach the stable state, but the final state is the same as that of I_1.

Since the external input does not affect the shape of the final state, but rather selects which state is produced, we can build a degree of invariance in the system since a shifted, rotated or scaled version of a stored image can recall the stored image. The effect of such distortions of the input image is to decrease the level of the initial condition. As long as the initial condition is above the loop threshold (θ in Fig. 8(b)), the loop is always brought to the stable state that is most similar to the initial input. This means that the dynamics is determined by the relative position of the initial input with respect to the loop threshold. The initial condition is determined by the degree of distortion of the external image as well as its light intensity. On the other hand, the loop threshold is determined by system parameters such as the neural gain and loop loss. In the next section we give experimental results of system invariances against various distortions. The problem of how to select optimal system parameters to make the trade-off between distortion tolerance and capability of recognizing correct images will be presented in Section 5.

4.2 Retrieval of the Complete Image from a Distorted Input

In this section we show experimental results of the invariance property of the memory loop in recognizing a distorted image. The images stored in the loop are the four faces shown in Fig. 7(a). They are recorded as a Fourier-transform hologram as described in Section 3.

Fig. 11(a) shows the response of the memory when the half face of a recorded image is presented to the system with the loop shutter **OFF**. This sets the initial condition of the loop. We then turn the loop shutter **ON** to close the feedback loop. The signal then circulates in the loop and the state evolves. After many iterations the loop reaches the stable state and the complete face appears. The time for this process ranges from less than one second to several seconds, depending on the initial conditions and the system parameters. The complete image is locked in the loop even after the external input is

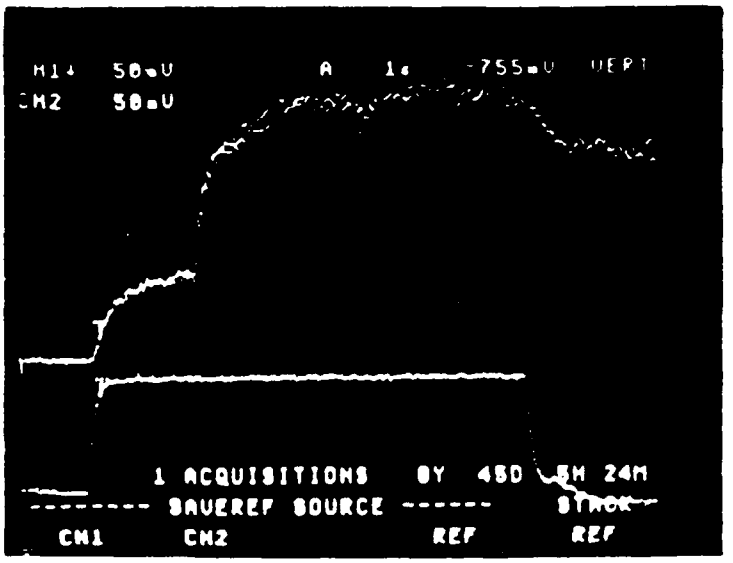

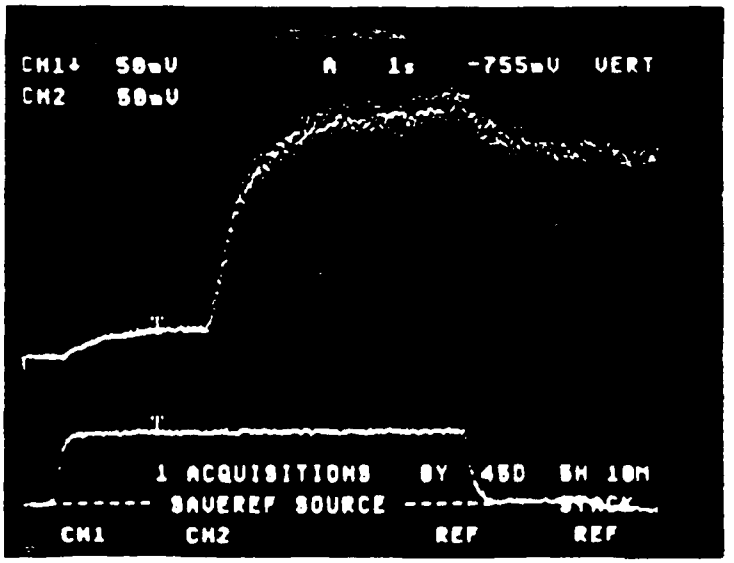

Fig. 9: Temporal Response of the Loop. (a) Strong input. (b) Weak input. Timing: t_1 = Input ON, t_2 = Feedback ON, t_3 = Input OFF.

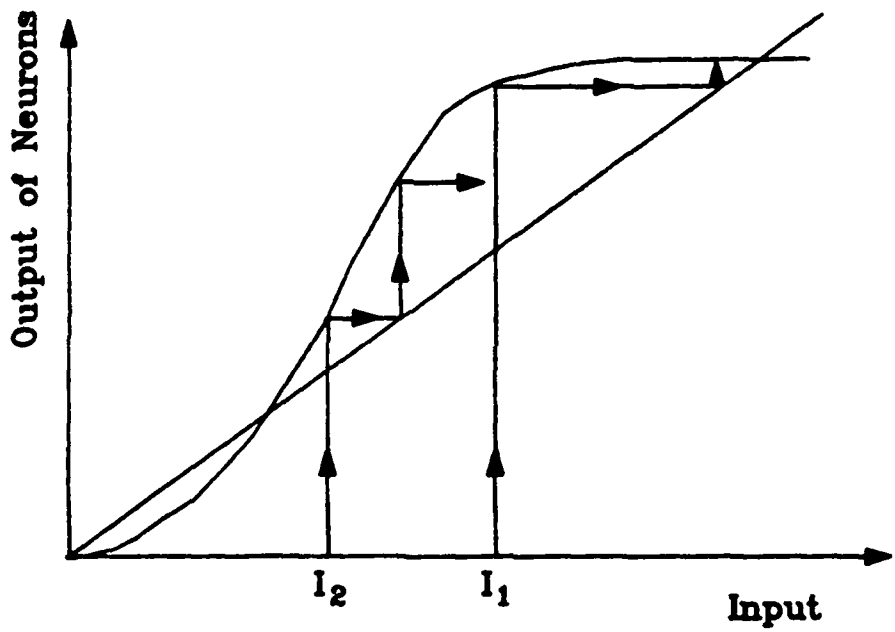

Fig. 10: Convergence of the Loop.

turned **OFF**. Fig. 11(b) shows the system output at the moment the loop shutter is **ON**. We see that the feedback image is superimposed on the external input. Fig. 11(c) shows the output 0.4 seconds after the feedback loop is closed, and Fig. 11(d) shows the output 0.8 seconds after the feedback loop is closed. Fig. 11(e) shows the complete image recalled from the loop after 2 seconds. Fig. 11(f) shows that after we remove the external input the recalled image is latched in the loop. Fig. 12 shows the temporal sequence of the same experiment but with another half-face as the input. This experiment shows that the external input to the associative memory does not need to be exactly the same as the recorded images.

Now we use a rotated version of one of the stored images as the input to investigate the rotation invariance capability of the loop. Fig. 13(a) shows the response of the memory when a rotated version of a recorded image is presented into the system with the loop shutter **OFF**. The input is rotated by 6 degrees with respect to the original image. Fig. 13(b) shows the memory output at the moment the feedback loop is closed. The loop state then evolves to give the original image. The temporal sequence of this evolving is shown in Fig. 13(c) to Fig. 13(e). In this experiment the degree of rotation of the input image sets the initial condition of the loop. More rotation means more distortion; hence the initial condition is farther away from the stored memory. Thus, the loop needs more iterations to arrive at the stable state. Fig. 14(a) shows this result.

In the figure the upper curve represents the stable state intensity of the output image and the lower curve represents the time for the loop to reach stable states, both as a function of rotation angle. It shows that as the input is rotated, it takes a longer time to be recognized. However, *once the loop converges* to the stable state, the output intensity is always the same regardless of initial rotation. The figure also shows that the output intensity drops to zero when the initial input is rotated over 8 degrees. This means that the initial condition is below the loop threshold and the rotated image is not recognizable. One way to increase the tolerance of rotation is to increase the neural gain so that it can detect weaker feedback signals from the distorted input. Fig. 14(b) shows the result of the same experiment but with the neural gain 10 times higher compared to that used in Fig. 14(a). The rotation tolerance now increases to 16 degrees. One might infer that we can obtain more tolerance simply by increasing the neural gain. This is not true since high gain also enhances crosstalk and the loop may not converge to the correct image. This problem will be addressed in Section 5.

The third experiment on distortion tolerance is scale invariance. Fig. 15(a) shows the response of the memory when the scaled version of the face of a recorded image is presented to the system with the loop shutter **OFF**.

This face is 85% of the size of the original stored image. After we turn **ON** the feedback shutter, the loop evolves to the stable state. The temporal sequence of this evolving behavior is shown in Fig. 15(b) to Fig. 15(e). We now remove the external input by turning **OFF** the input shutter. Fig. 15(f) shows that the loop remains latched to the original image. The convergence time in this case is 1.5 seconds. This is longer than what would be required if the input were the original image. However, the two cases give the same output intensity. When the input image is further scaled down to 70% of the original size we need to increase the neural gain from 10^4 to 10^5 for the loop to recognize

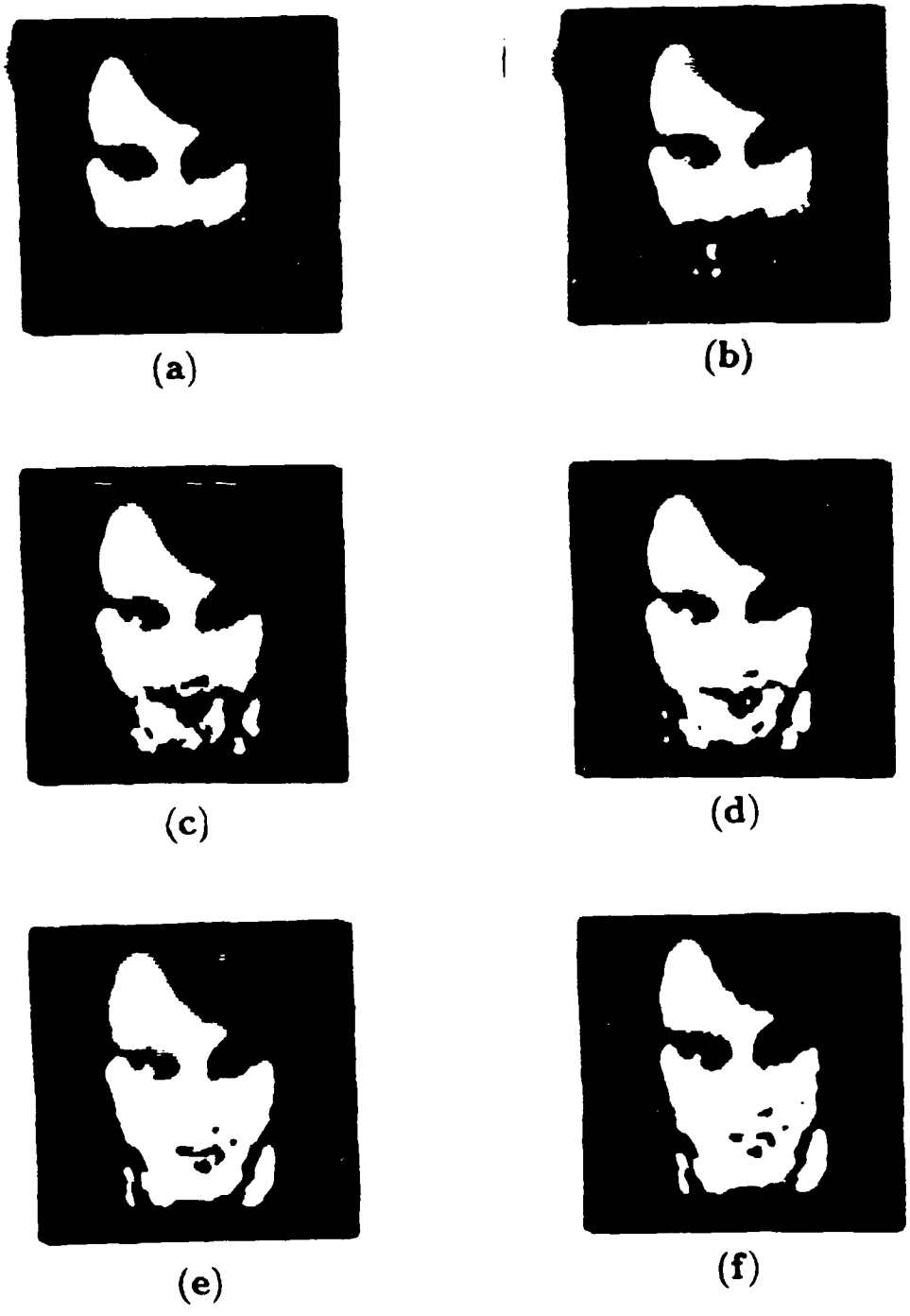

Fig. 11: Retrieval of the complete Image from the Partial Input. (a) The partial input at $t = 0$. (b) $t = 0^+$ (Loop closed). (c) $t = 400\ ms$. (d) $t = 800\ ms$. (e) $t = 2$ sec. (f) Input OFF.

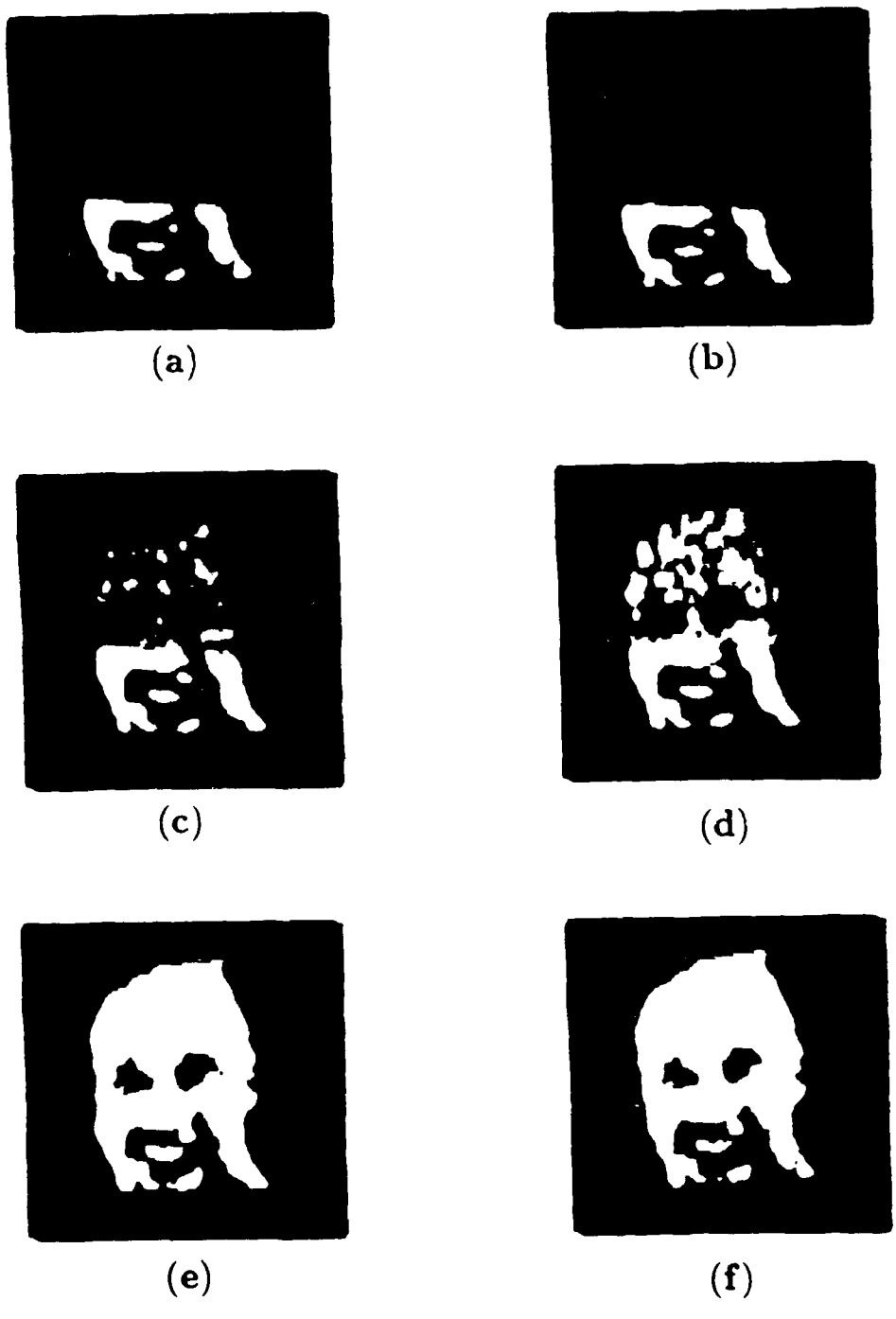

Fig. 12: Retrieval of the complete Image from the Partial Input. (a) The partial input at $t = 0$. (b) $t = 0^+$ (Loop closed). (c) $t = 480\ ms.$ (d) $t = 800\ ms.$ (e) $t = 2$ sec. (f) Input OFF.

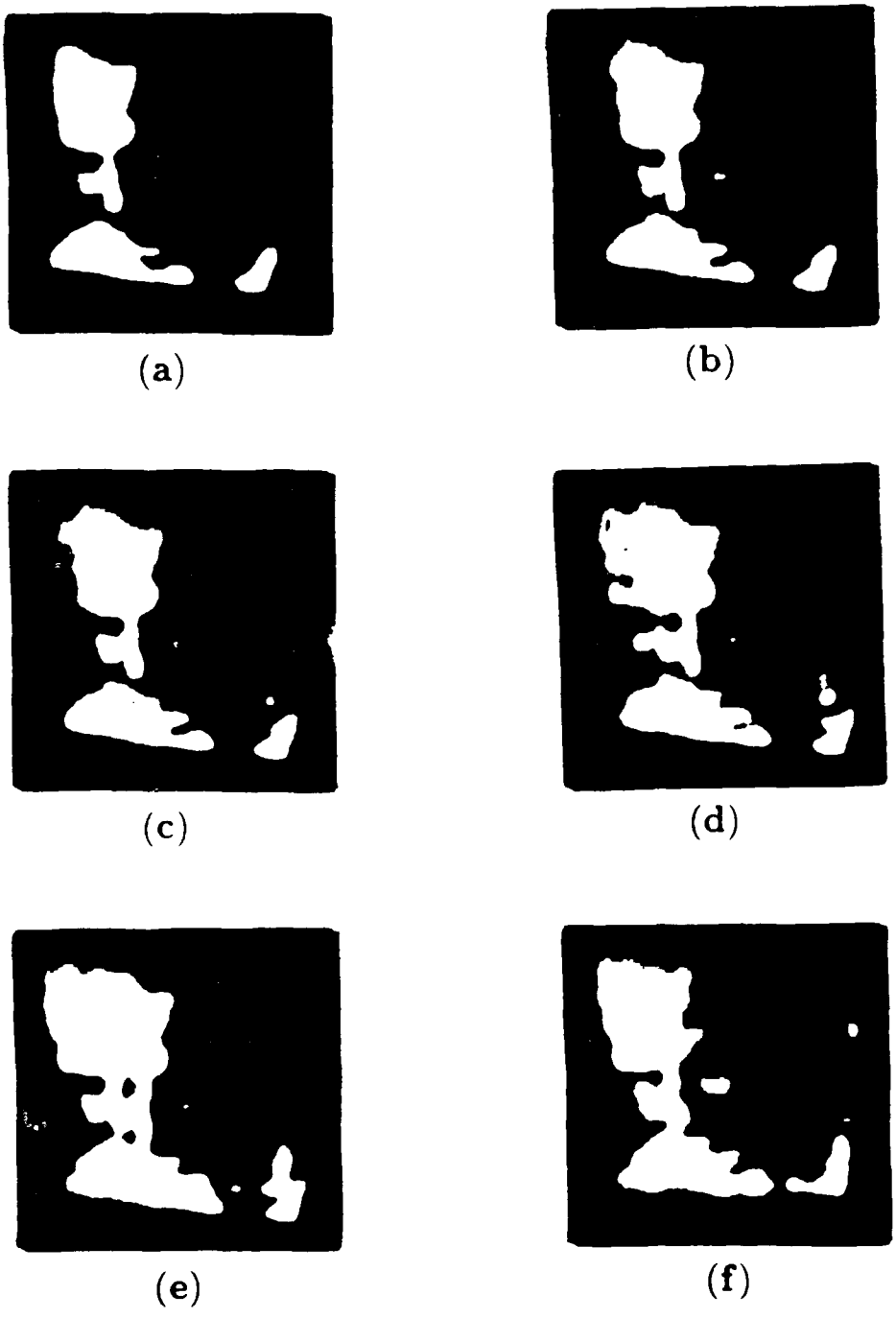

Fig. 13: Retrieval of the complete Image from the Rotated Input. (a) The input at $t = 0$. (b) $t = 0^+$ (Loop closed). (c) $t = 1.8$ sec. (d) $t = 3.6$ sec. (e) $t = 4.8$ sec. (f) Input OFF.

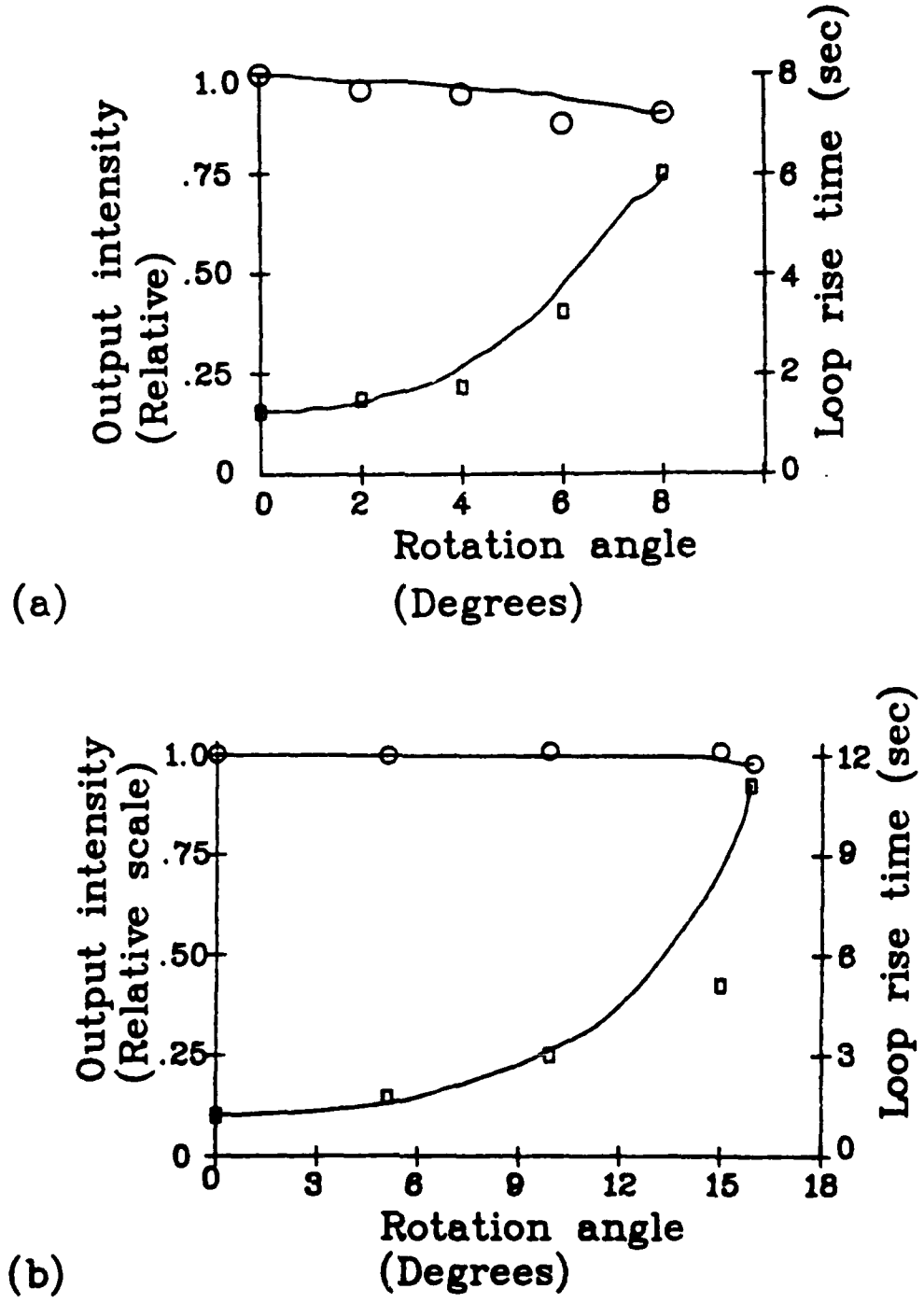

Fig. 14: Rotation Invariance Property of the Optical Loop. (a) Optical gain = 10^4. (b) Optical gian = 10^5. (o: Output intensity. ◇: Loop rise time.)

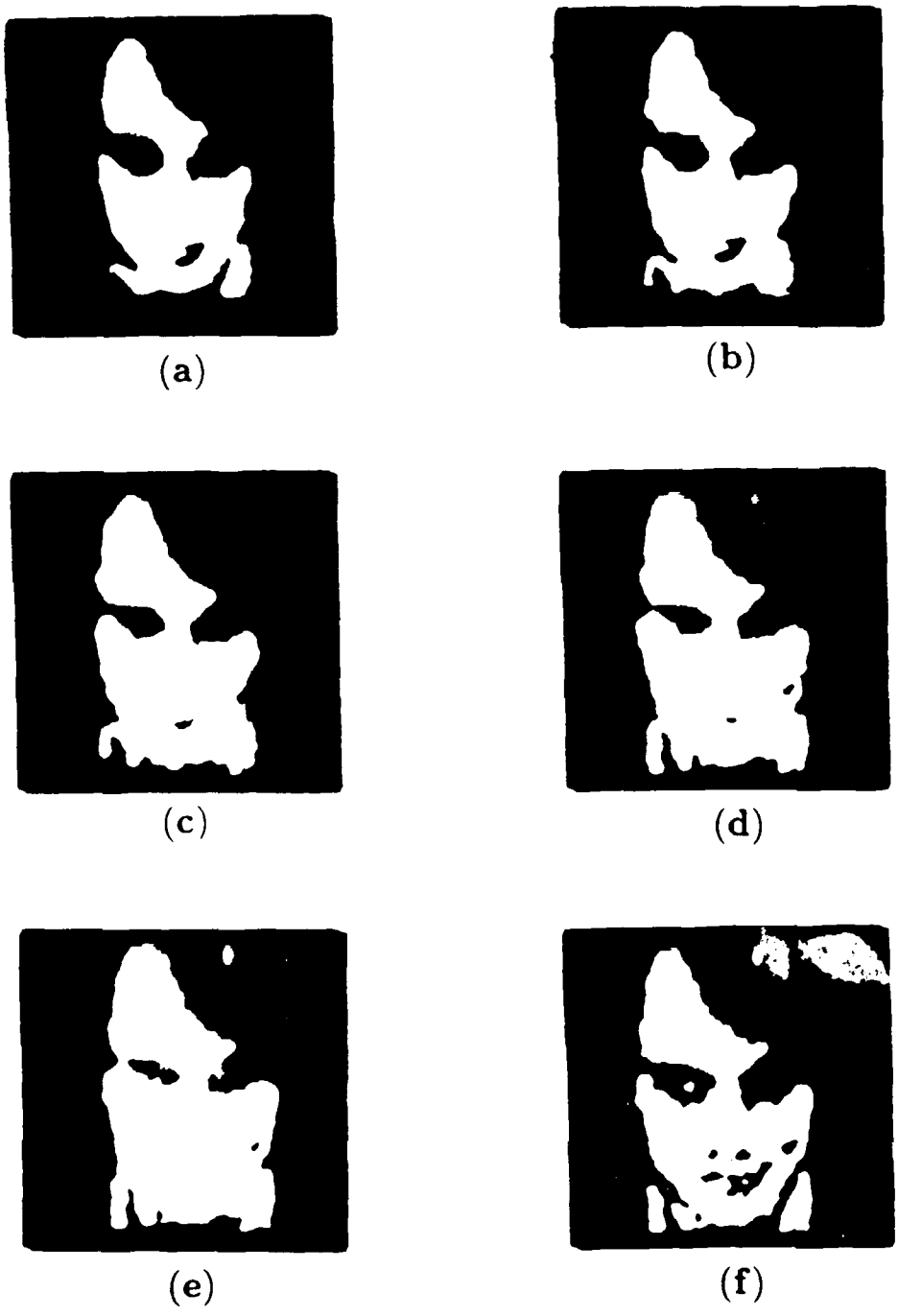

Fig. 15: Retrieval of the Complete Image from the Scaled Input. (a) The input at $t = 0$. Image size = 85%. (b) $t = 0^+$ (Loop closed). (c) $t = 1.8$ sec. (d) $t = 3.0$ sec. (e) $t = 4.8$ sec. (f) Input OFF.

the image. But this high gain results in low discrimination such that an input image that is not stored is also incorrectly recognized. These results are consistent with the dynamics and the invariance properties that we discussed above.

In principle, this loop is shift invariant since the images are stored in the Fourier-transform holograms. If one of the stored images appears at the input plane, there will be a bright spot at the correlation plane. If the input image shifts, the correlation peak will also shift to a corresponding position. However, if the peak shifts out of the pinhole position, then we lose the feedback signal and the image cannot be latched in the loop. Only when the shift equals an exact image spacing can the correlation peak pass through the pinhole to close the feedback path. But then the image that appeared in the window would be different from the previous one. Hence, this loop is shift-invariant only within the pinhole size. Without the pinholes the cross-correlation noise and the auto-correlation peak would be fed back to the loop together and the reconstructed images would not be recognizable. There is a compromise between pinhole size and loop performance. Small pinholes allow good memory discrimination and sharp reconstructed images, but can also cut the signal to below the level that can be detected by the threshold device and reduce the shift tolerance of the system. The function of the pinhole array in this system might also be met by using a nonlinear spatial light modulator, in which case we can achieve full shift invariance [18, 19].

Fig. 16(a) shows the read-out image from the LCLV, which comes from an external input shifted away from its stored position. This shift moves its correlation peak so that it does not match the position of the pinhole. Thus, there is no feedback signal going through the loop. If we cut off the input image, the read-out image will die out with a characteristic time of about 50 to 400 ms, corresponding to the response time of the LCLV. Now we shift the input image around, trying to search for the correct position. Once the input image comes close enough to the correct position, the correlation peak passes through the right pinhole, giving a strong feedback signal superimposed with the external input on the neurons. The total signal then goes through the feedback loop and is amplified continuously until the neurons are saturated. Fig.s 16(b) to (e) show the temporal sequence of this development from the moment that a sufficient portion of the correlation peak passes through the pinhole to the complete recall of the original image. Fig. 16(f) shows the image in the loop with the input turned **OFF** and the memory latched. In this experiment the pinhole diameters are 90 μm. As long as the correlation peak is close enough to the pinhole, the original image can be recalled. Depending on how far the input image is shifted from the original position and the optical gain of the neurons, the time required for the loop to reach a stable state is between two to several seconds. The lower curve of Fig. 17(a) shows the loop rise time as a function of shift when the neural gain is 10^4.

The upper curve shows the output intensity as a function of shift. It shows that the shift tolerance for this particular image is 220 μm and that the loop converges to the image with the same intensity. If the shift is more than 220 μm, the feedback signal is too weak to trigger the loop and the output is zero. If we increase the neural gain by a factor of ten, then the shift invariance increases to about 500 μm. This is shown in Fig. 17(b). However, sidelobes are also amplified in the loop; hence the image may be uncorrectly recognized.

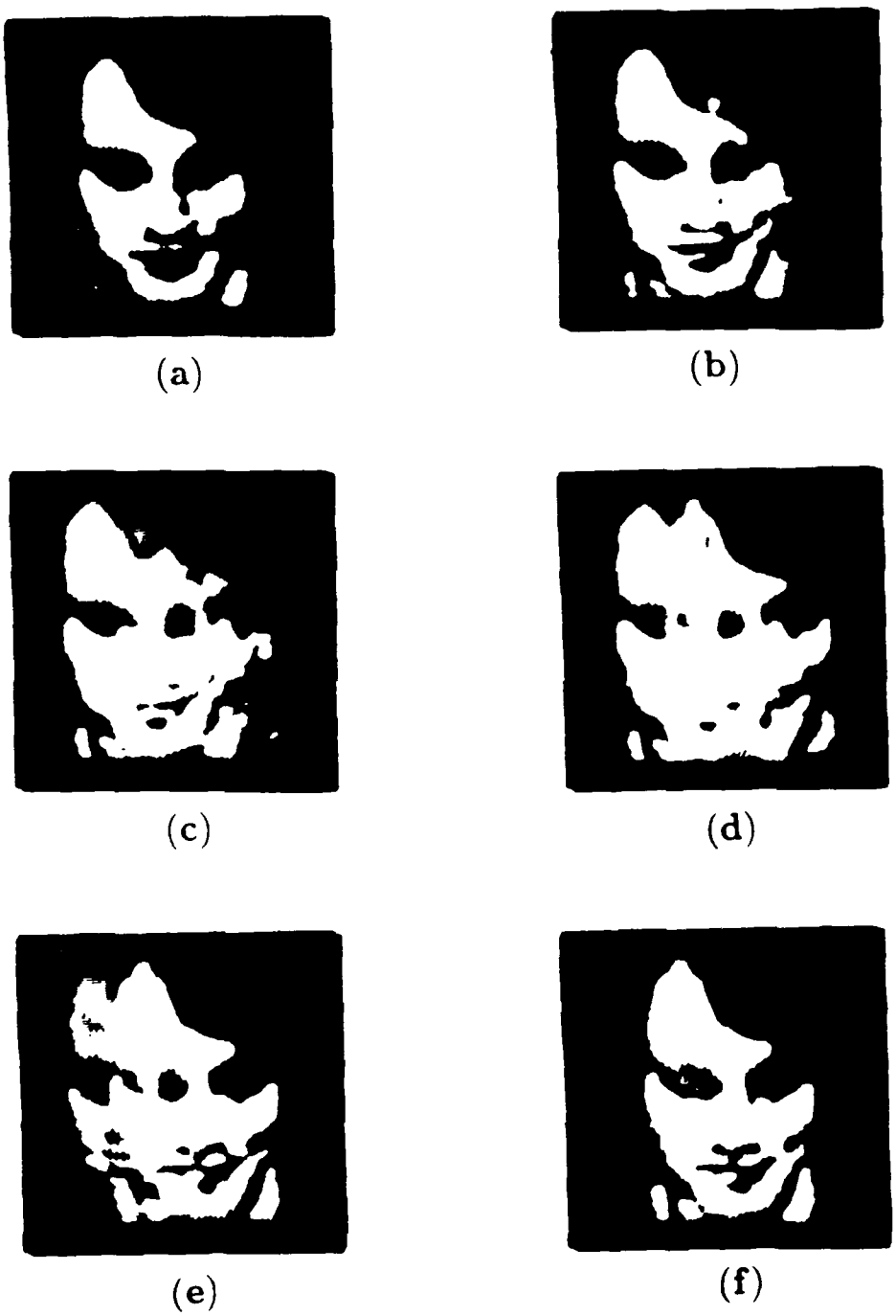

Fig. 16: Retrieval of the Complete Image from the Shifted Input. (a) The input at $t = 0$. (b) $t = 0^+$ (Loop closed). (c) $t = 2.4$ sec. (d) $t = 3.0$ sec. (e) $t = 0.4$ sec after the input is OFF. (f) Stable state.

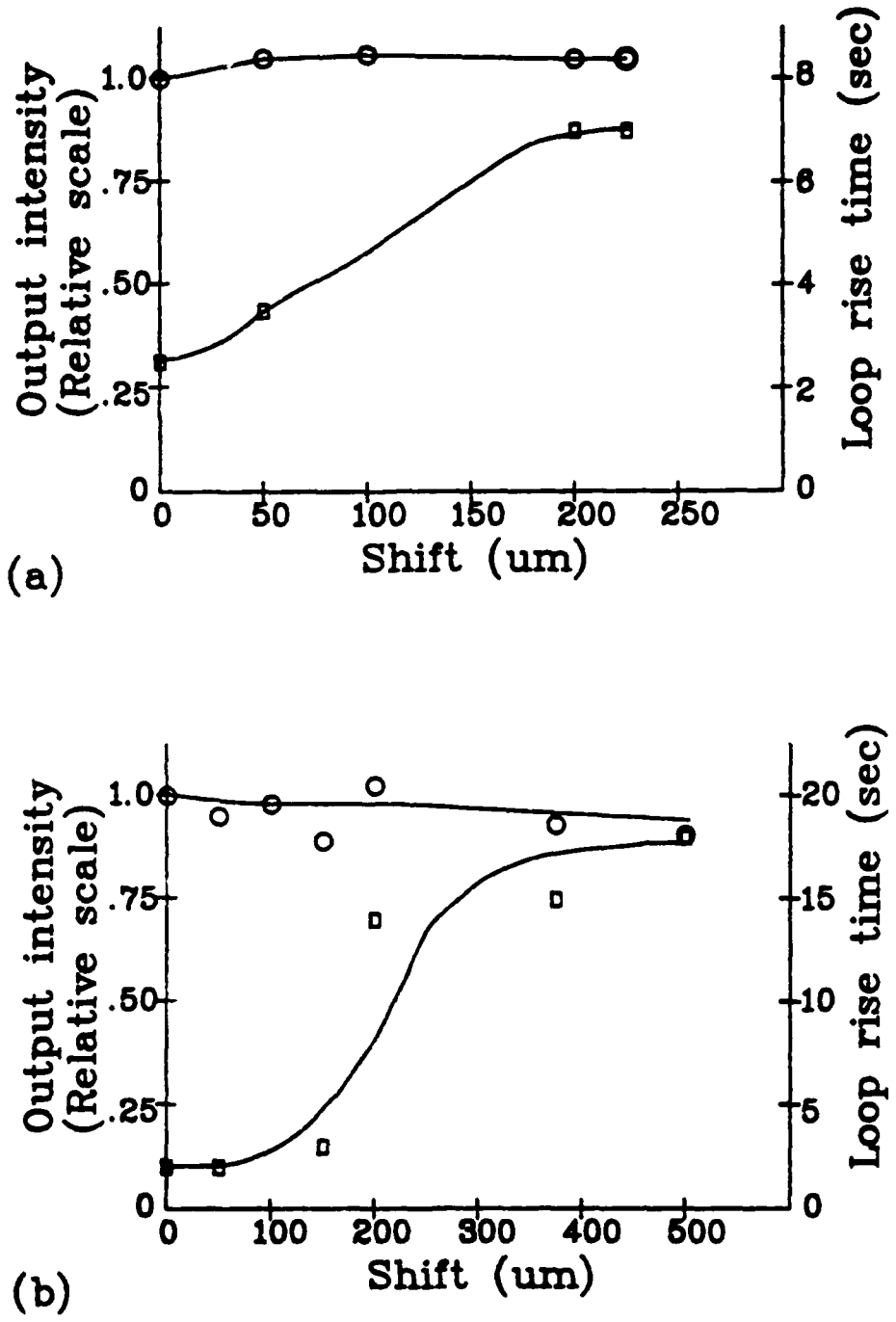

Fig. 17: Shift Invariance Property of the Optical Loop. (a) Optical gain = 10^4. (b) Optical gian = 10^5. (o: Output intensity. ◇: Loop rise time.)

The dynamic and invariance properties of the associative loop shown above imply that the associative memory has error-correcting capability, since the input does not have to be the same as the original memory to be recognizable. We show this capability particularly by using four words as memory. Fig. 18(a) shows the four words recorded in the Fourier-transform holograms of our system. Fig. 18(b) shows an input word that has three spelling errors. However, it has four correct letters, **O, P, I, A**, at the correct positions. Hence the correlation of (**OP4I&A**) with the memory gives sufficient feedback signal to trigger the loop iterations. Fig. 18(c) shows the word recalled from the loop, superimposed on the input. Fig. 18(d) shows the loop latched to the correct word after the input is turned **OFF**. If we increase the neural gain, the loop would be able to recognize more erroneous words. But then it will lose the discrimination capability because a completely different word would also induce enough feedback for the word to be recognized as one of the stored words.

5 Trade-Off Between Distortion Tolerance and Discrimination Capability

The experimental results shown in the above subsection demonstrates the distortion-invariance capability of the associative loop. The input images do not have to match the memory exactly. Furthermore, by raising the neural gain, no matter how much we change the initial condition by rotating, shifting, and scaling the input image, the loop can always be made to produce an image as a stable state. But the ability to correctly recognize a stored image from a distorted input and the discrimination capability, i.e., the ability to distinguish images from one another, compromise each other. If there is too much gain, then just shining a flashlight at the input of the system causes it to lock on to one of its stable states. If the gain is set too low, then even an input that is a slightly distorted version of one of the stored images is not recognizable. In particular, there are two parameters under our control that can affect the gain in the loop: The gain of the neurons and the size of the pinholes.

The importance of selecting an optimal neural gain can be explained by the loop iteration map. Fig. 19 shows the iteration map of a low gain loop. In the figure there is no intersection between the gain curve and the loss line, and the gain curve is always below the loss line. Therefore, no matter how well the input image matches the stored images and no matter how bright the correlation peak is, the output of the neuron is always below the loss line. Hence, the loop signal becomes weaker and weaker in successive iterations until finally it decays to zero. Fig. 20(a) shows the response of the loop to an input image, with the feedback shutter **OFF**. Fig. 20(b) and (c) shows the output after the loop is closed. Fig. 20(d) and (e) shows the loop output after the input image is **OFF**. The loop image decays because the neural gain is too low.

On the other hand, too much neural gain also causes problem. Fig. 21 shows the iteration map with high gain. In this figure the gain curve is higher than the loss line and they intersect at a low value. Hence, the loop has a low threshold. Therefore, a small correlation signal is enough to trigger the loop to evolve. As shown in the above subsection, this loop can tolerate more image distortions such as rotation, scaling, shift, etc., and can still recognizethem. This means that the loop has a very large radius of attraction for each memory state. However, it also means that its discrimination capability to distinguish different images is poor. It is quite possible that the loop recognizes other images as one of

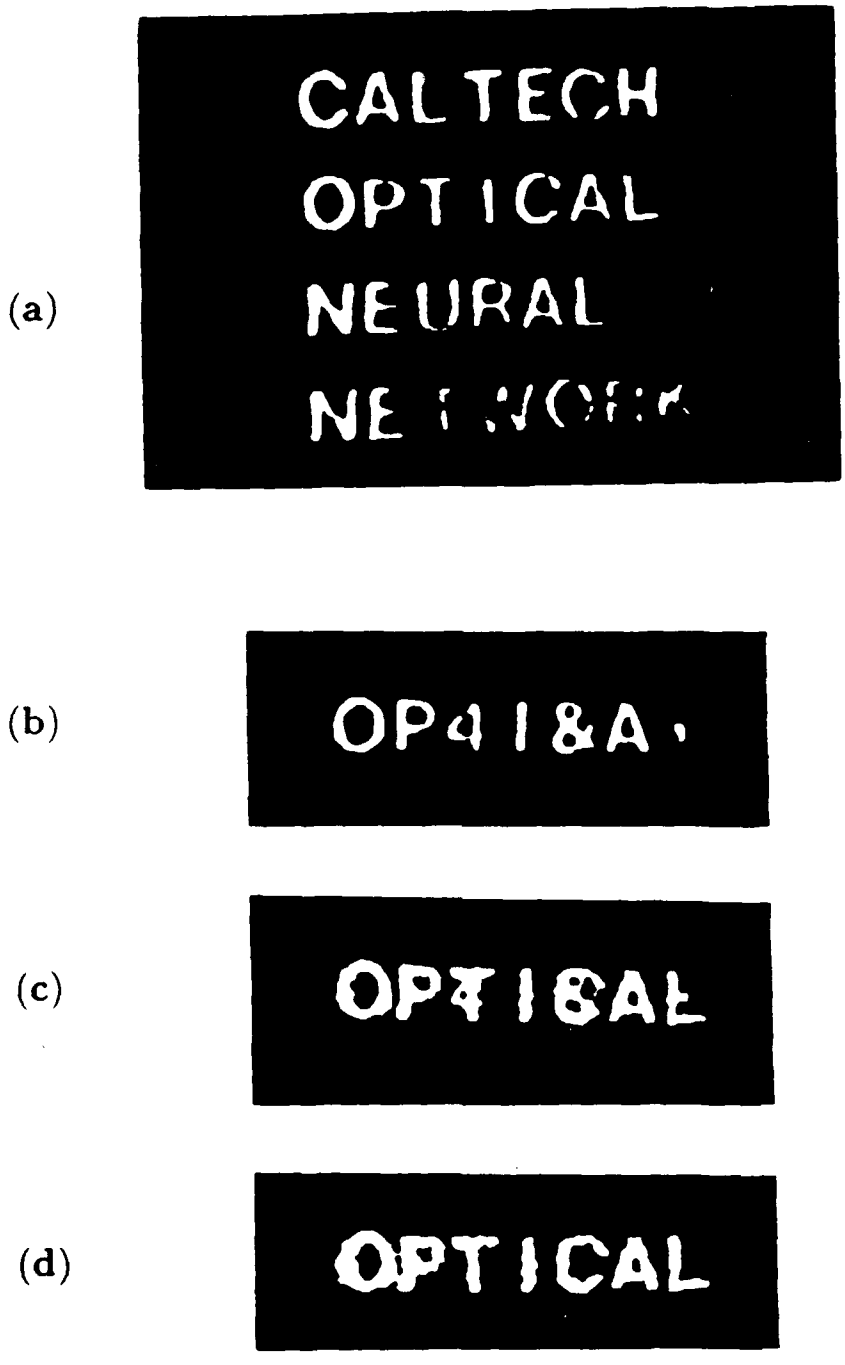

Fig. 18: Error-Correction Capability of the Loop. (a) The stored images. (b) External input with errors. (c) Feedback image superimposes with the input image. (d) The stable state of the loop after the external is OFF.

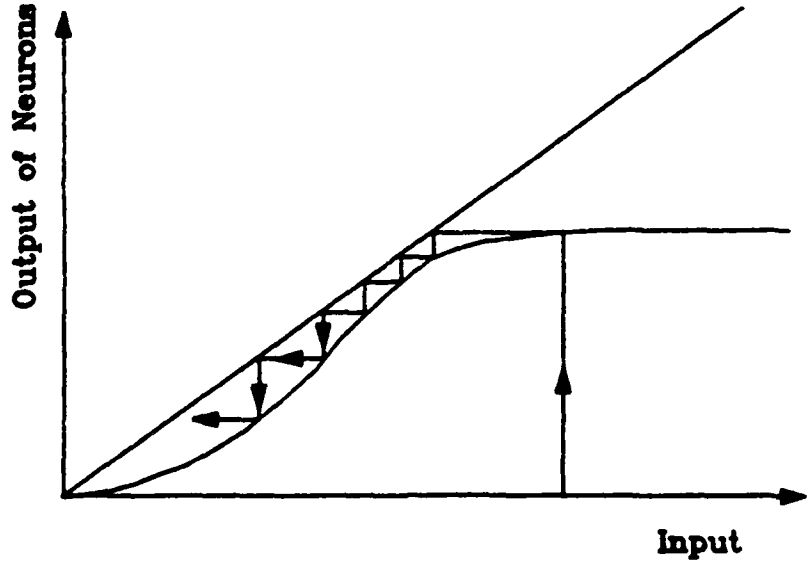

Fig. 19: Iteration Map of Low Optical Gain.

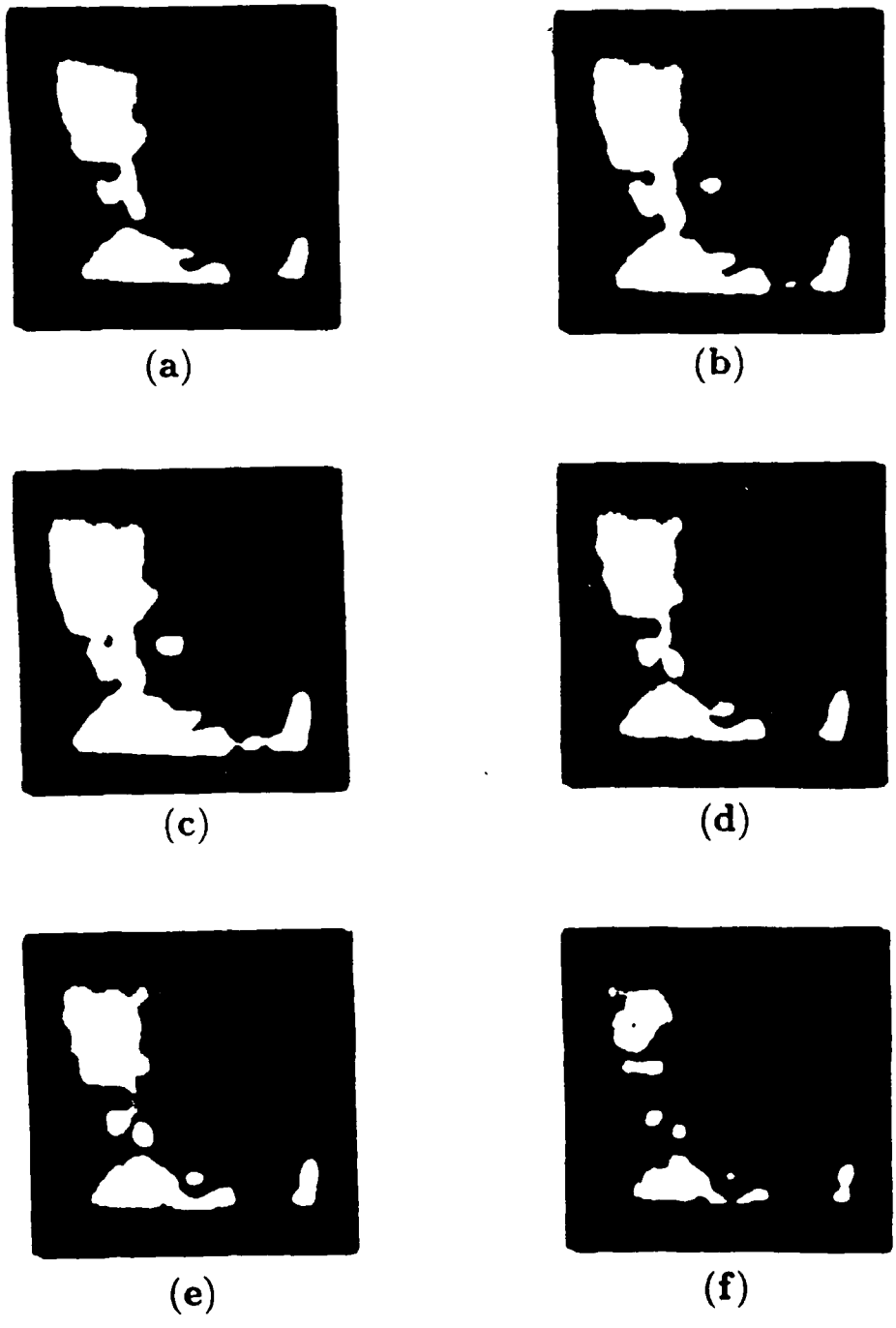

Fig. 20: Loop dynamics of Low Optical Gain. (a) The input at $t = 0$. (b) $t = 0^+$ (Loop closed). (c) $t = 3$ sec. (d) @ Input OFF. (e) $t = 1.2$ sec after the input is OFF. (f) $t = 1.8$ sec after the input is OFF.

the stored images. Fig. 22(a) shows an image that is not stored in the memory. Fig. 22(b) to (d) show that the unfamiliar image triggers the loop to evolve after the feedback shutter is turned **ON**. Fig. 22(e) shows that after the input image is turned **OFF**, the loop is locked to one of the stored images. This shows the loop making an incorrect recognition.

The gain required to sustain the iteration loop is determined by the loop loss. The factors in this system that decide the loss are the pinhole size, the hologram diffraction efficiency, and the reflections from optical components. Among them the pinhole size is the key factor since the other components are generally fixed. We use Fig. 3 as an example. Let $f_i(x,y), i = 1,2,3,4$, represent the images of the letters **A, B, C, D**, respectively, and let the pinhole size be W. Then the reconstructed images in the window at P_1 can be shown to be

$$\sum_{i=1}^{4}[g_{1i}(x,y)\mathrm{rect}(\frac{x}{W})\mathrm{rect}(\frac{y}{W})] * f_i(x,y) \tag{17}$$

where $\mathrm{rect}(\frac{x}{W})\mathrm{rect}(\frac{y}{W})$ represents the finite size of the pinholes, * represents the convolution operation, $g_{11}(x,y)$ the auto-correlation of **A**, and $g_{1i}, i \neq 1$, the cross-correlations of **A** with **B, C, D**, respectively. We see that the images are blurred by the finite dimension of the pinholes. Decreasing W gives better image quality, but we need to increase the gain of the neurons to compensate for the loss caused by the small pinholes. At the other limit, if the pinhole size is increased, we do not need very high-gain neurons but the image quality deteriorates. Fig. 23 shows the effect of the pinhole size on the stable-state loop images. In the limit where W becomes infinitely large, the reconstructed image in the window at P_1 becomes a superposition of all the stored images, each approximately equally strong, and severely blurred. Fig. 24 shows the temporal sequence of the loop signal under the condition of infinite pinhole size. It is seen that final image in the loop is totally unrecognizable.

Thus, there is an optimum pinhole size and an optimum neural gain. Fig. 25 shows the experimental results of minimum gain required and maximum gain allowable for the loop to sustain a stable memory as a function of pinhole size. Below the minimum gain the loop can not recognize any image in the sense that once the external input is cut off, the loop activity decays to zero. Above the maximum gain the loop loses discrimination capability such that any input image, even a flashlight, will trigger the loop into a stable state. Note that the minimum gain increases when the pinhole size is increased to more than 250 μm. This is because the reconstructed images are blurred so much that the correlation peaks are weakened and the losses in the loop are increased. Fig. 25 shows that the optimum pinhole size in this system is in the range of 70 μm to 150 μm. We choose 90 μm for most of the experiments. Although this measurement is particular for the images we used, the above behavior is true in general.

6 Neural Network Model for the Memory Loop

The architecture of the optical associative memory that we presented in the preceding sections is a Hopfield-type network. In the system, the neurons are simulated by the LCLV, and the interconnections between the neurons are achieved by holographic gratings. In the following, we present an analysis of the neural network model of thc optical associative-memory loop. Based on the model, we will discuss the convergence properties of the system

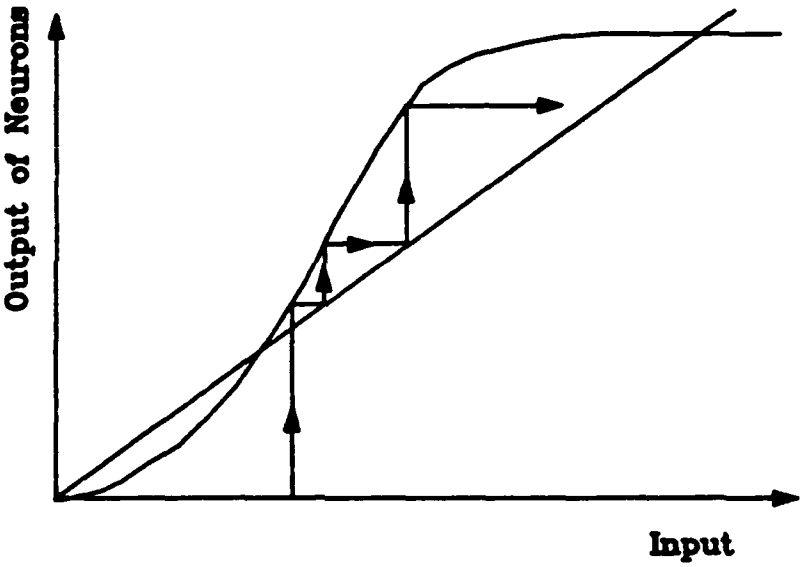

Fig. 21: Iteration Map of High Optical Gain.

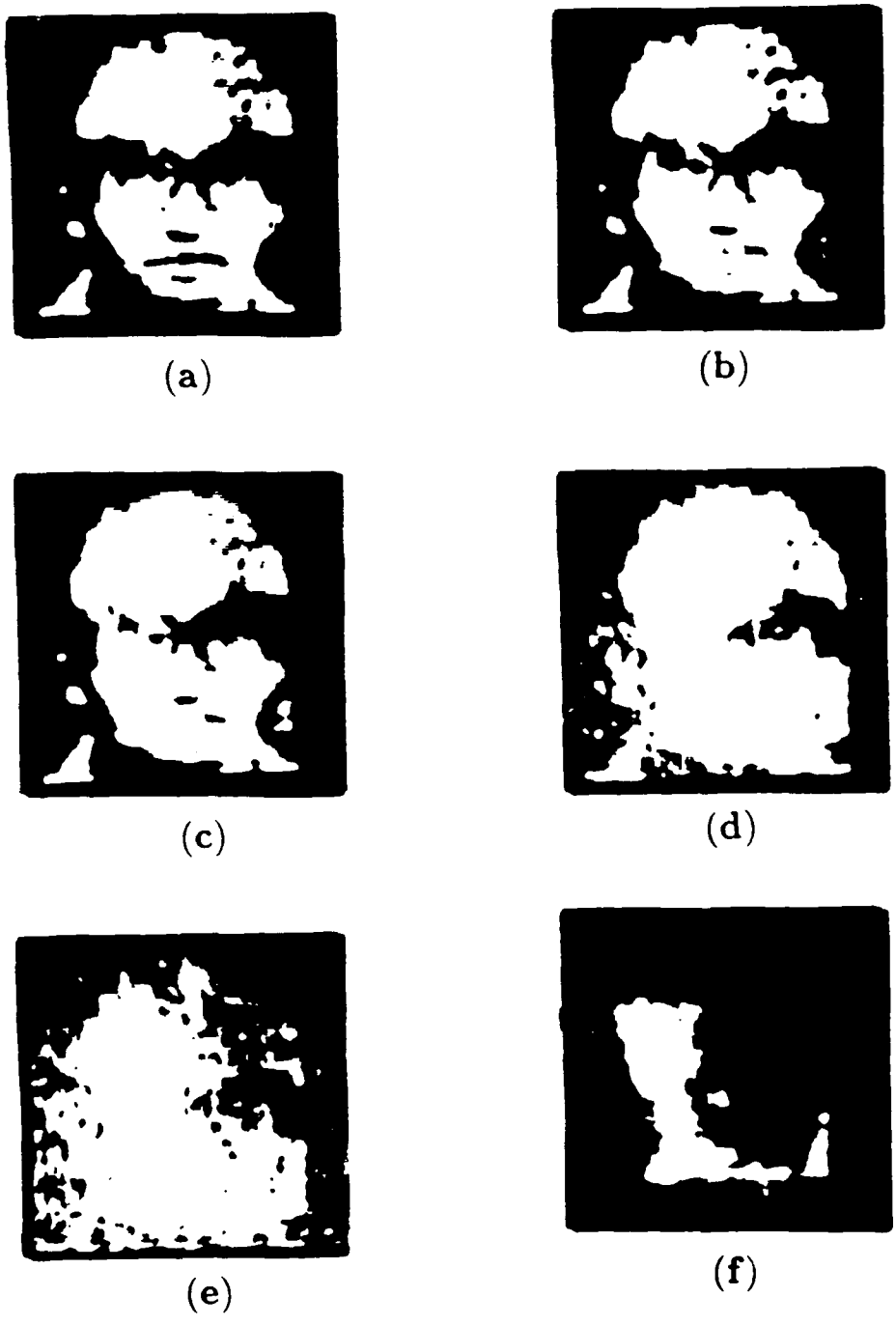

Fig. 22: Loop dynamics of High Optical Gain. (a) The input at $t = 0$. (b) $t = 0^+$ (Loop closed). (c) $t = 1.2$ sec. (d) $t = 1.8$ sec. (e) The input is OFF. (f) Stable state.

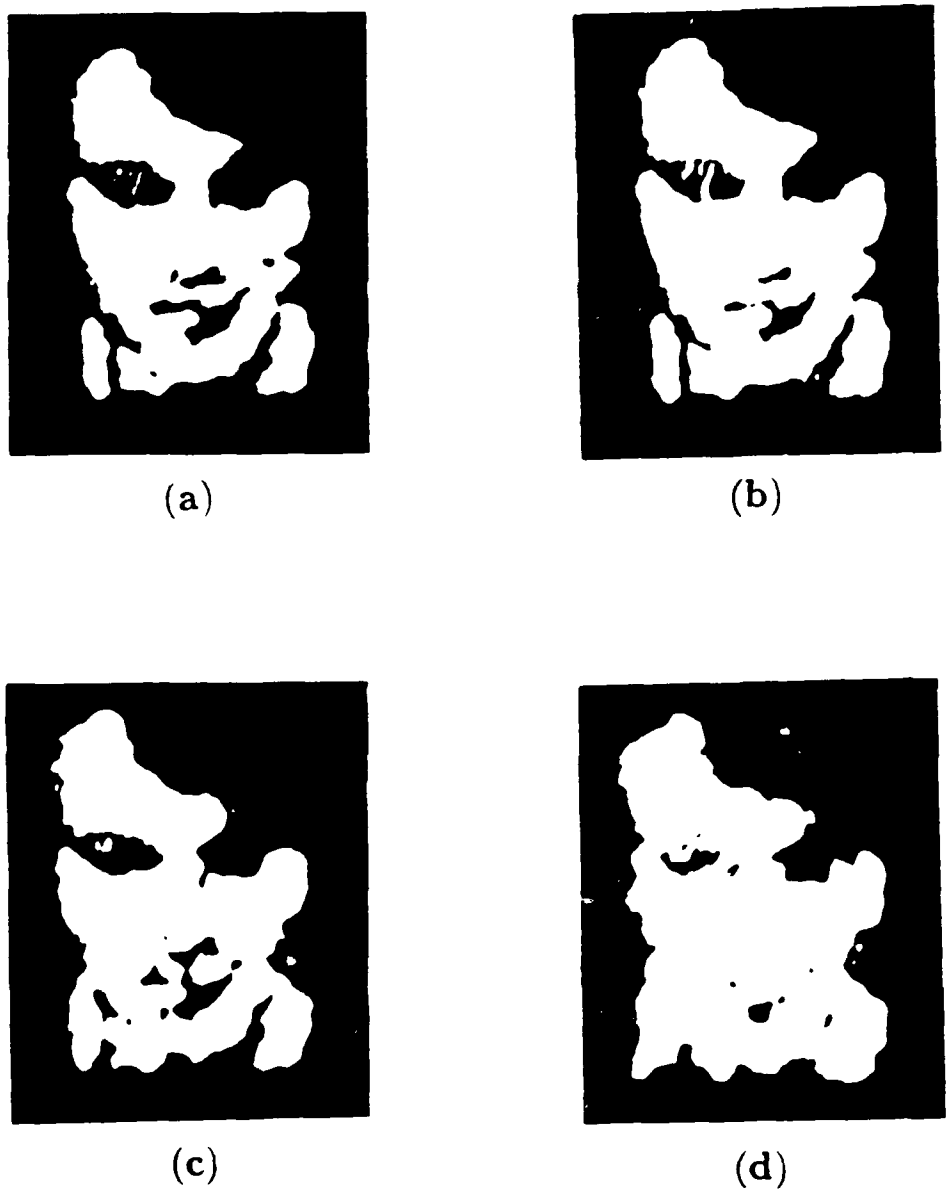

Fig. 23: Output Image for Different Pinhole Sizes. (a) 40 μm. (b) 90 μm. (c) 180 μm. (d) 400 μm.

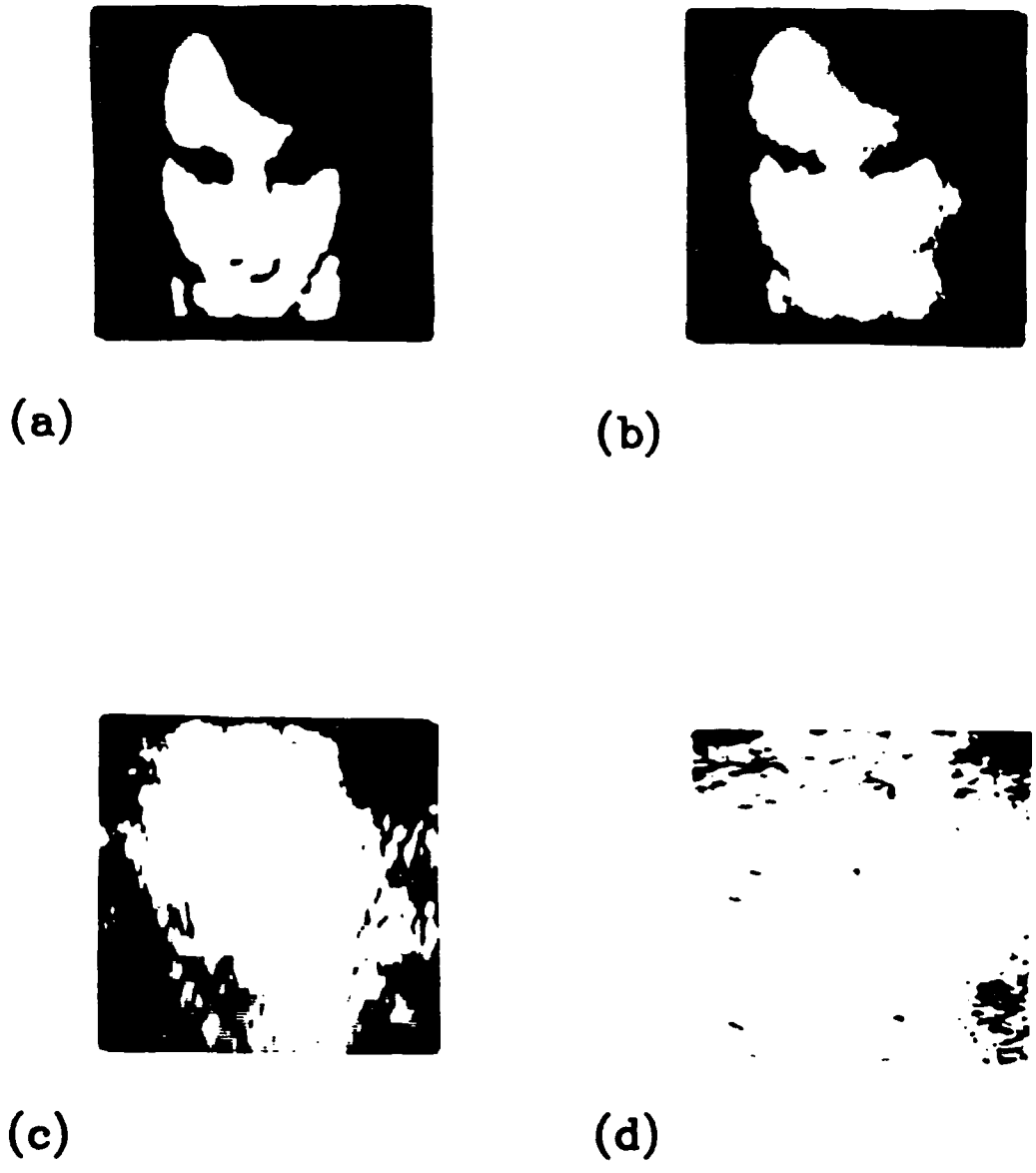

Fig. 24: Loop Behavior without the Pinholes. (a) The input at $t = 0$. (b) $t = 0^+$. (Loop closed). (c) $t = 0.6$ sec. (d) $t = 2$ sec

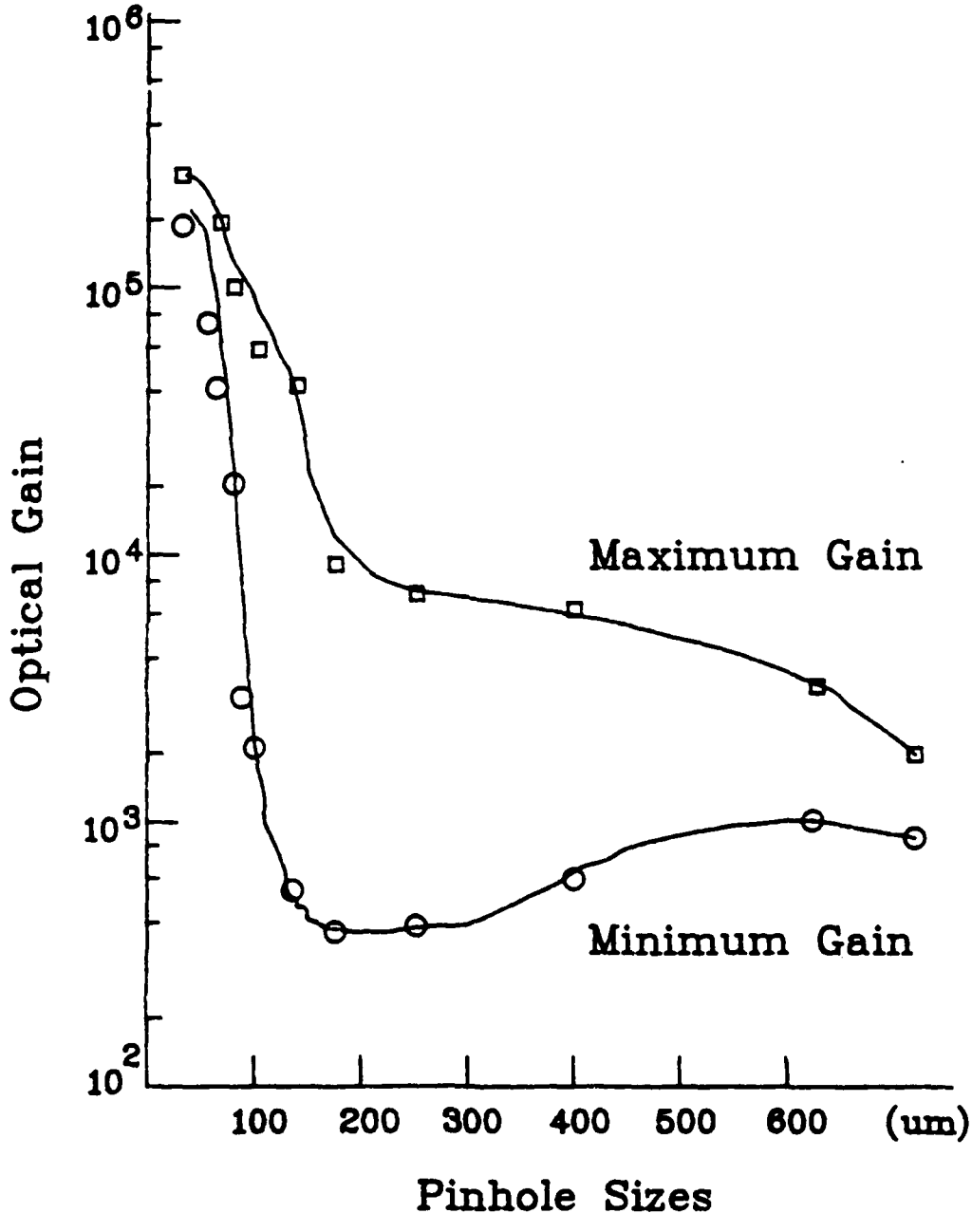

Fig. 25: Optimum Pinhole Size and Optical Gain.

and the stability of the stored memories.

Recall from Eq. 16 that the feedback signal of each iteration in the optical loop can be written as

$$f^o(x,y,t) = \sum_{m=1}^{M} (f \star f^m)(0,0,t)\, f^{m*}(x,y), \tag{18}$$

where $f^m(x,y)$ ($m = 1 \ldots M$) are the stored images, $f(x,y)$ is the input image to the LCLV, $\star$ is the cross-correlation operator, and f^{m*} is the complex conjugate of f^m. Eq. 18 shows that the feedback signal in the loop is the superposition of the reconstructed images from the second hologram, each being weighted by the cross-correlation of the input with the images stored in the first hologram. In the optical system, we make the first hologram H_1 with high-pass characteristics. The high-pass Fourier-transform hologram was obtained by adjusting the ratio of the recording intensities of the reference beam and the object beam such that the high-frequency part has good modulation depth while the low-frequency parts were overexposed. Thus, in reconstruction there is no diffraction from low-frequency gratings, and only high-frequency components reconstruct the image. The reconstructed image contains only the edges of the original image, as was shown in Fig. 7(b). The characteristics of the high-pass hologram can be described by subtracting the low-frequency portion from the original spectrum, which can be represented approximately by removing the dc signal. Using the high-pass hologram as H_1 in the optical loop, the cross- correlation term $f * f^m$ in Eq. 18 now should be replaced by the convolution of the input $f(x,y)$ with the stored images $g^m(x,y)$, i.e., $f \star g^m$, where $g(x,y)$ is the high-pass version of $f(x,y)$. Since $g^m(x,y)$ is the original image with the dc level removed, it can be described by

$$g^m(x,y) = f^m(x,y) - \iint f^m(\xi,\eta)\, d\xi\, d\eta, \tag{19}$$

where the integration is performed over the finite size of the images.

Instead of taking continuous functions $f^m(x,y)$, $f(x,y)$, etc., we will approximate by sampling discrete points (pixels), indexed by i, j, etc. (The number of the sampled points N should be greater or equal to the SBP of the optical system.)We can approximate $(f \star g^m)(0,0)$ by summation of the inner product

$$(f \star g^m)(0,0) = \sum_{l=1}^{N}\sum_{k=1}^{N} f_{lk} g^m_{lk} \tag{20}$$

and write

$$g^m_{lk} = f^m_{lk} - \frac{1}{N^2}\sum_{i,j=1}^{N} f^m_{ij}. \tag{21}$$

The feedback signal can thus be written as

$$\begin{aligned} f^{(o)}_{ij} &= \sum_{m=1}^{M}\Big[\sum_{l=1}^{N}\sum_{k=1}^{N} f_{lk} g^m_{lk}\Big] f^{m*}_{ij} \\ &= \sum_{l=1}^{N}\sum_{k=1}^{N} w_{ij;lk}\, f_{lk}, \end{aligned} \tag{22}$$

where

$$w_{ij;lk} = \sum_{m=1}^{M} g_{lk}^{m} f_{ij}^{m*}$$
$$= \sum_{m=1}^{M} [f_{lk}^{m} - (\frac{1}{N^2} \sum_{l,k=1}^{N} f_{lk}^{m})] f_{ij}^{m*}. \quad (23)$$

Note that the matrix W is nonsymmetric and that its diagonal terms are not zero in this case.

For simplicity of discussion, we use one-dimensional signals in the following analysis. The extension to the two-dimensional case is straightforward. We also assume that the signals are real. In fact, this may not be true in the real system, because the nonuniformity and phase distortions of the optical components and the LCLV may cause signals to become complex. However, the analysis then becomes difficult if we try to take this into account. Furthermore, the intensity of the signal is detected in each iteration, and the phase information does not accumulate in the system; thus, our assumption is reasonable. Following these arguments, the w_{ij} for the 1-D case is modified as

$$w_{ij} = \sum_{m=1}^{M} (x_j^m - a_m) x_i^m, \quad (24)$$

where

$$a_m = \frac{1}{N} \sum_{j=1}^{N} x_j^m \quad (25)$$

is the average level of image m. The feedback signal shown in Eq. 22 can then be written as

$$y_i = \sum_{j=1}^{N} w_{ij} x_j. \quad (26)$$

Therefore, the feedback signal after one cycle and before thresholded by the neurons can be obtained by inserting Eq. 24 into 26, which gives

$$y_i = \sum_{j=1}^{N} \Big(\sum_{m=1}^{M} (x_j^m - a_m) x_i^m \Big) x_j$$
$$= \sum_{m=1}^{M} \Big[\Big(\sum_{j=1}^{N} x_j^m x_j \Big) - \Big(\sum_{j=1}^{N} x_j \Big) a_m \Big] x_i^m. \quad (27)$$

Note that in this case the x_i^m and x_j are unipolar, i.e., 0 or 1; whereas y_i can be biploar because w_{ij} is bipolar. The above expression can be written in a matrix form,

$$\mathbf{y} = \sum_{m=1}^{M} \Big[\Big(\mathbf{x} \cdot \mathbf{x}^m \Big) - \Big(\sum_{j=1}^{N} x_j \Big) a_m \Big] \mathbf{x}_m. \quad (28)$$

The signal $\mathbf{y}$ is fed back at the neuron plane and is thresholded by the neurons to give the signal for the next iteration. Thus, the new signal for the next iteration is

$$\mathbf{x} = g(\mathbf{y}). \tag{29}$$

This process then repeats until the loop reaches an equilibrium state. Clearly, if we want to investigate the equilibrium states and the stability characteristics, we should solve the dynamic equations of the system. However, before we go to that step, we can qualitatively predict the performance of the loop simply by inspecting the physical meaning of each term of the feedback signal.

As is seen in Eq. 28, the total feedback signal is the weighted sum of the stored images $\mathbf{x}^m$. The weight of each $\mathbf{x}^m$ is determined by the two terms in the square bracket. The term $\mathbf{x} \cdot \mathbf{x}^m$ is the cross-correlation of the input $\mathbf{x}$ and the stored image $\mathbf{x}^m$, while $\sum_{j=1}^{N} x_j$ is the dc level of the signal $\mathbf{x}$, and a_m is the dc level of the stored image $\mathbf{x}^m$. The subtraction of the product of the dc levels from the correlation signal gives the weight. Thus, only the pixels that have correlation with the stored $\mathbf{x}^m$ sufficiently larger than the dc levels contribute a significant component to $\mathbf{y}$. Therefore, only the strongest stored image component that appears in $\mathbf{x}$ will be enhanced in the feedback, while weaker components are suppressed by subtracting the average image. This argument suggests that the loop will work as an associative memory.

In the case of the optical loop, the neural gain is the main factor that determines whether the loop can recall a correct memory state. The modeled network shows the same behavior. To illustrate this point, we perform simulations with different gains. Fig. 26 shows an example of computer simulation. There are three patterns stored in the high-pass network; each pattern has a 30 pixels. In the figure, the height at each position represents the signal strength of that pixel. When a partial $\mathbf{x}^2$ is input into the system, it converges to a stable state that is closest to the $\mathbf{x}^2$ after 160 iterations. As the gain is reduced, the loop takes more iterations to reach the steady state. However, when the gain is reduced to below a certain level, the loop can no longer sustain the loop signal and the signal gradually decays to zero. This is illustrated in Fig. 27. On the other hand, as the gain is increased, the loop evolves to a steady state in fewer steps. But if the gain is too high, the loop converges to a mixed state of the stored images, which may be very distorted and unrecognizable. Fig. 28 shows simulations under high-gain conditions. The results of these simulations show that the modeled network has the same characteristics as the optical loop: It has the capability of recognizing distorted images, but there is a trade-off between distortion tolerance and discrimination capability, which is governed by the neural gains.

Note that in the simulation of Fig. 26 the steady-state image of the loop is slightly different from the original images. But we still consider it a correct recall. Here the *correct* memory means that it has a *similar* shape as the original image, although there is a slight distortion and the signal level is weaker. The reason for that distortion is easily understandable by inspecting Eq. 27. We see that the feedback contains not only the autocorrelation signal, but also the cross-correlations with all other memories. Depending on the values of the cross-correlation and the gain function, some of the crosstalks will be detected by the neurons and survived in the loop; thus, the total output is distorted. The

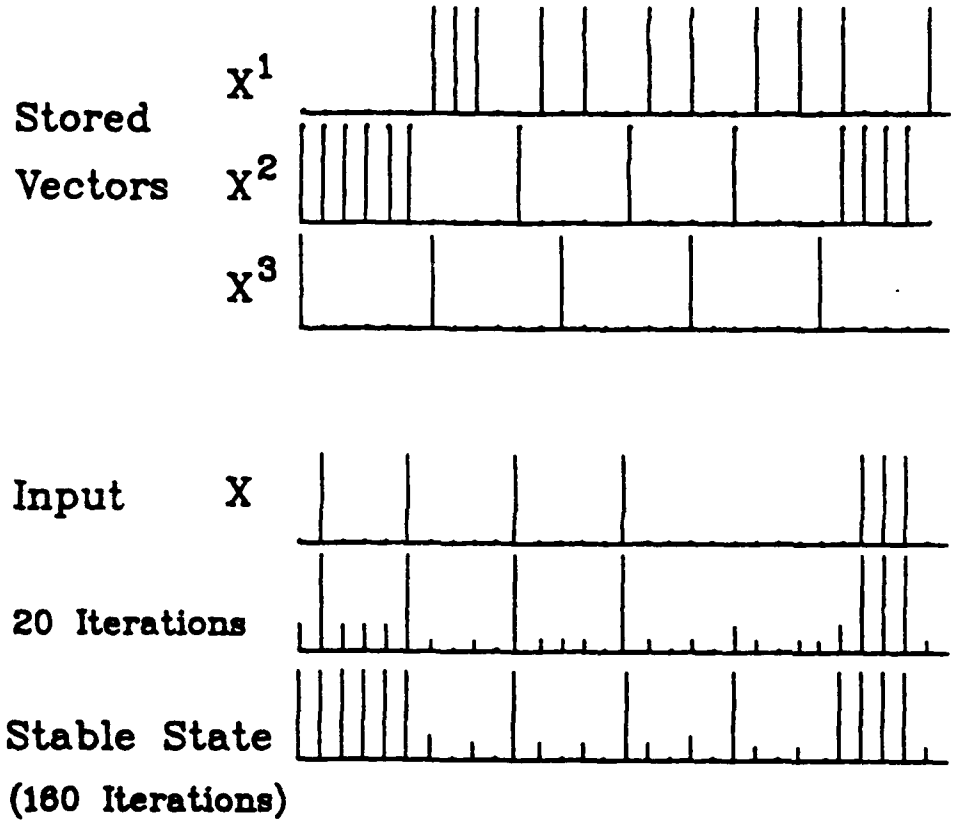

Fig. 26: The dynamics of the high-pass loop with a good gain.

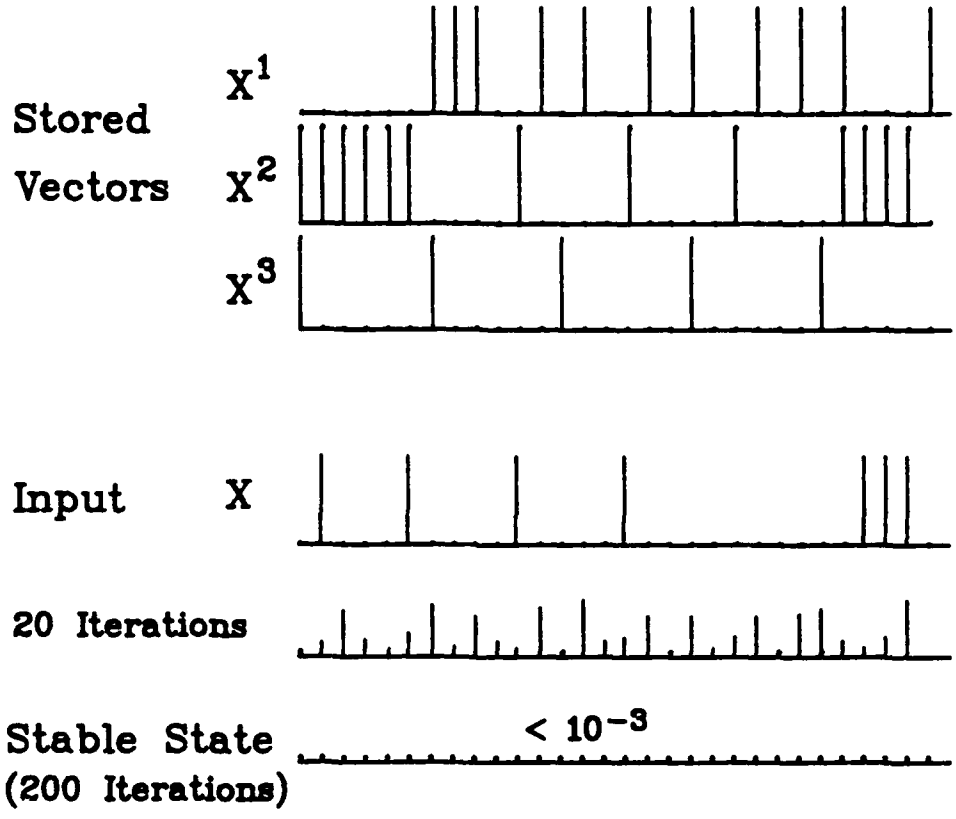

Fig. 27: The dynamics of the high-pass loop with a low gain.

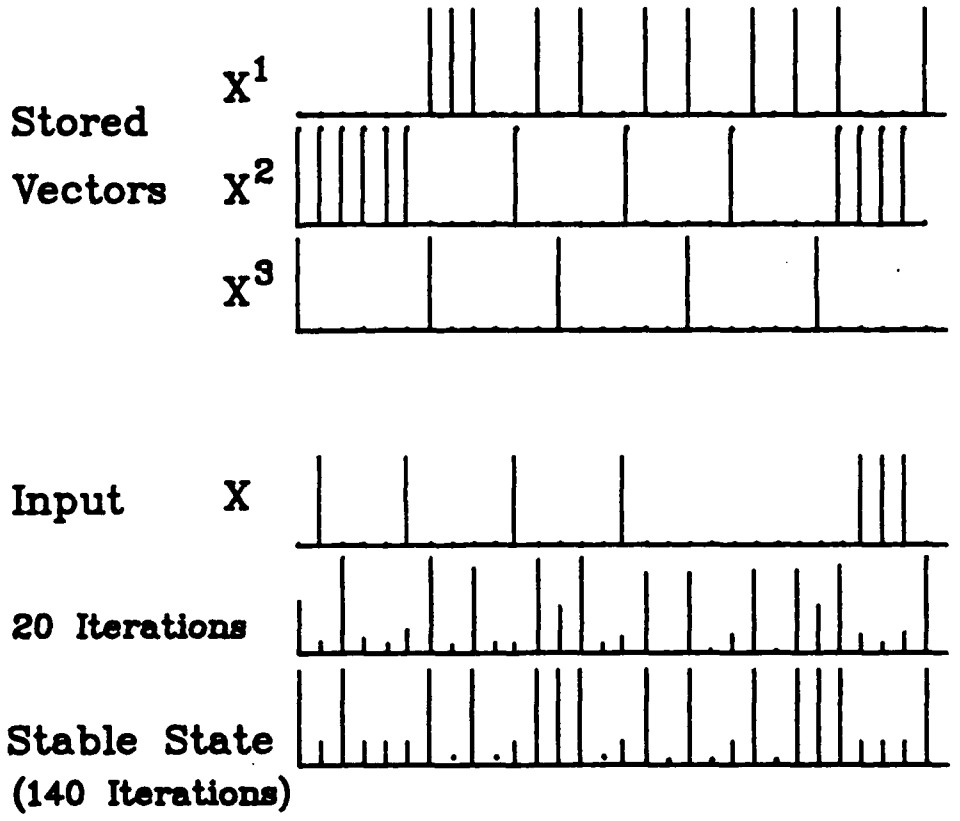

Fig. 28: The dynamics of the high-pass loop with a high gain.

higher the neural gain the worse the distortions. We will return to this point later when we examine the steady-state solution of the dynamic equations of the system.

An interesting question that we want to address is whether the high-pass hologram is necessary and how it affects the system performance. Suppose the first hologram is not a high-pass version, then the interconnection strength can be obtained by setting $a_m = 0$ in Eq. 24. We get

$$w_{ij} = \sum_{m=1}^{M} x_i^m x_j^m. \tag{30}$$

Similarly, the feedback signal can be obtained by setting $a_m = 0$ in Eq. 28,

$$\mathbf{y} = \sum_{m=1}^{M} \Big(\mathbf{x} \cdot \mathbf{x}^m\Big)\mathbf{x}_m. \tag{31}$$

The feedback signal now is simply the superposition of the stored images each being weighted by the cross-correlation of the input image and the stored images. The strongest correlation gives the strongest feedback signal and it determines the state to which the loop will most possibly converge. Hence the loop still works as an associative memory. However, because there is no mechanism to suppress the crosstalks, noise is also easily picked up by the neurons. The discrimination capability of the loop will be poorer than the high-pass loop. Fig. 29 shows an example of the computer simulation. The images used in the high-pass simulations are used here. Simulations show that as long as the stored images have crosstalks, then the low-pass loop always converges to a mixed state. There is only a very narrow range of the gain where the system gives the correct output. Therefore, the high-pass hologram is very crucial in the performance of the loop.

To this point, we have developed a neural network model of the optical associative loop, and we have investigated its characteristics with computer simulations. Results show that the model matches well with the optical loop. However, the above treatment is not very rigorous and does not show the dynamic behavior of the system. Therefore, it is not completely satisfactory. In general, only the solution of the dynamic equations can fulfill our purpose.

In our system, an optical neuron is simulated by one pixel of the LCLV, which gives response x_i to its input y_i. The dynamics of the neuron is described by the following equation

$$\frac{dx_i}{dt} = -x_i + g(y_i), \qquad i = 1 \ldots N, \tag{32}$$

where $g(y_i)$ is a nonlinear function describing the neuron response. To complete the feedback loop, we substitute the expression of Eq. 26 into Eq. 32, we obtain

$$\frac{dx_i}{dt} = -x_i + g\Big(\sum_{j=1}^{N} w_{ij} x_j\Big), \qquad i = 1 \ldots N \tag{33}$$

where w_{ij} is the high-pass version of the interconnection strength given by Eq. 24. This is the equation describing the dynamics of the optical loop. In what follows, we will discuss

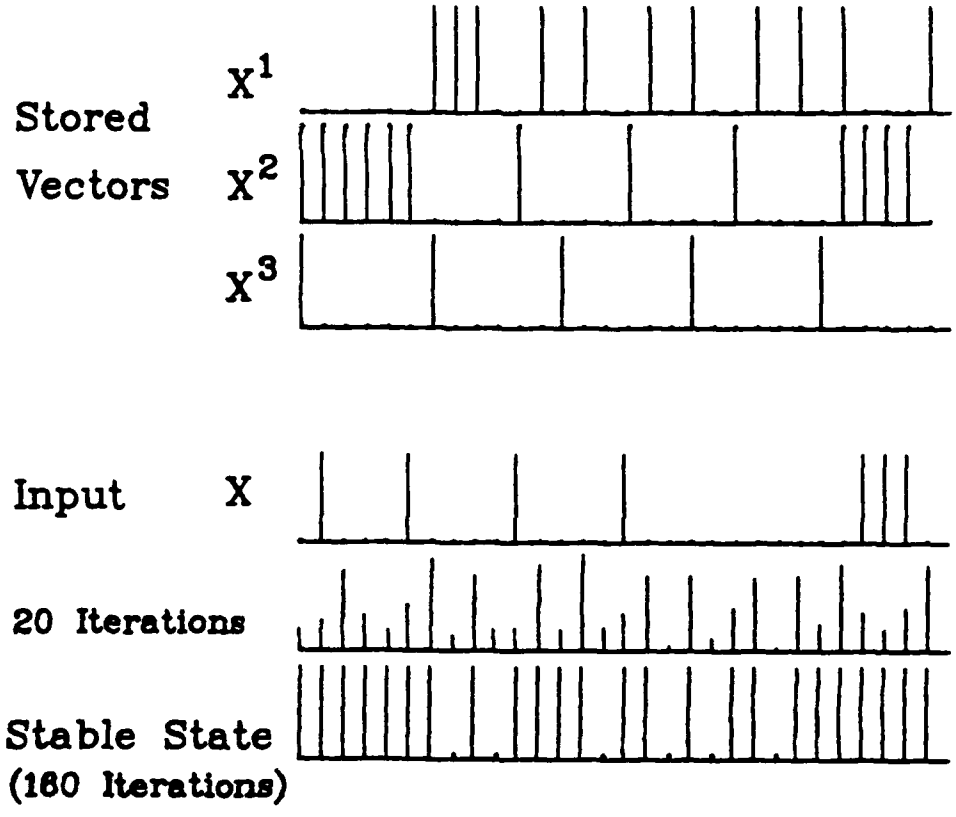

Fig. 3.29: The dynamics of the loop without the high-pass filter.

the system's, dynamics using a geometrical method [20]. The main idea of the method is that corresponding to each set of stored memories we first define a new vector space; then the dynamic equations are transformed consequently into this space and the dynamics can be observed as a phase flow on the hyper-surface. We assume that the stored images $\mathbf{x}^1 \ldots \mathbf{x}^M$ are linearly independent. This is reasonable since the number of pixels in the image, N, is usually much larger than M, and we are not considering the trivial case where one of the stored images is a linear combination of the others. Since the stored images are linearly independent, they span a vector space $\mathbf{V_1}$. Then, we can form a vector space $\mathbf{V_2}$ that is orthogonal to $\mathbf{V_1}$ such that the N-dimensional vector space $\mathbf{R}^N$ is the direct sum of the two sub-vector spaces; i.e.,

$$\mathbf{R}^N = \mathbf{V_1} \oplus \mathbf{V_2} \tag{34}$$

It is shown in the Appendix that we can derive a reciprocal basis $\beta_1 = \{\mathbf{y}^1 \ldots \mathbf{y}^M\}$ from $\{\mathbf{x}^1 \ldots \mathbf{x}^M\}$ for V_1, and an orthonormal basis $\beta_2 = \{\mathbf{y}^{M+1} \ldots \mathbf{y}^N\}$ for V_2 such that $\beta_1 \cup \beta_2 = \beta$ forms a basis for $\mathbf{R}^N$. Then any vector in $\mathbf{R}^N$ can be expressed as a linear combination of $\mathbf{y}^l, l = 1, \ldots N$.

It is shown in the appendix that the N-coupled differential equations of Eq. 33 can be represented in terms of the β coefficients as

$$\frac{dx_i}{dt} = -x_i + g\Big(\sum_{m=1}^{M} c_m x_i^m\Big) \qquad i = 1, \ldots, N. \tag{35}$$

Note that there are N-coupled differential equations, but there are only M parameters of c_m for all the equations. It is also derived in the appendix that Eq. 35 in turn can be transformed into two sets of equations

$$\frac{dc_l}{dt} = -c_l + \sum_{i=1}^{N} (x_i{}^l - a_l) g\Big(\sum_{m=1}^{M} c_m x_i{}^m\Big) \qquad l = 1, \ldots, M, \tag{36}$$

$$\frac{dc_l}{dt} = -c_l + \sum_{i=1}^{N} (y_i{}^l - b_l) g\Big(\sum_{m=1}^{M} c_m x_i{}^m\Big) \qquad l = M+1, \ldots, N \tag{37}$$

where

$$b_l = \frac{1}{N} \sum_{j=1}^{N} y_j{}^l. \tag{38}$$

Several comments can be made on Eq. 36 and 37. First, we see that the components c_1, ..., c_M are coupled together, but they are de-coupled from the components c_{M+1}, ..., c_N. On the other hand, the driving forces for c_{M+1}, ..., c_N depend only on c_1, ..., c_M. This means that the dynamics of the system are completely determined by c_1, ..., c_M, although c_{M+1}, ..., c_N are not necessarily zero. Therefore, we only need to study the dynamics of these M components. The equilibrium states can be obtained from Eq. 35, by letting $d/dt = 0$, we get

$$x_i = g\Big(\sum_{m=1}^{M} c_m x_i^m\Big). \tag{39}$$

We see that the equilibrium states are indeed determined by $c_1, \ldots, c_M$. Each of these c_m represents the component of the high-pass version of the input vector on the reciprocal vectors of the m^th stored image, which in some sense is proportional to the correlation between $\mathbf{x}$ and $\mathbf{x^m}$. The stored images which have stronger correlation give stronger components to the equilibrium image. Note that if the neurons are sensitive enough, they will also pick up weak cross-correlation components. Therefore, the output image will not be exactly the same as the stored images. However, the summation of all components from the stored images is thresholded by the neurons. Thus, the nonlinear gain function provides an enhancement of the closest stored image. This effect helps the network converge to the state near the stored images.

In principle, the dynamics of the system and its convergence properties can be obtained by solving Eq.s 36 and 37. In practice, it is impossible to obtain explicit solutions. In what follows we present a geometrical method to illustrate how the system evolves to a stable state, and how it is influenced by the parameters such as gain and initial conditions. In order to illustrate the concept, we will consider the case where only two images, $\mathbf{x^1}$ and $\mathbf{x^2}$, are stored in the memory. As we shall see, the two-image case contains all the salient features of the dynamics. As discussed in the previous paragraph, we need only to solve two dynamic equations in the two-image case. By Eq. 36, we have

$$\frac{dc_1}{dt} = -c_1 + \sum_{i=1}^{N}(x_i^1 - a_1)g(c_1x_i^1 + c_2x_i^2) \tag{40}$$

$$\frac{dc_2}{dt} = -c_2 + \sum_{i=1}^{N}(x_i^2 - a_2)g(c_1x_i^1 + c_2x_i^2). \tag{41}$$

Recall that a_1 and a_2 are the average levels of the input images $\mathbf{x^1}$ and $\mathbf{x^2}$. Let $h_1(c_1, c_2)$ represent the summation term in Eq. 40, and $h_2(c_1, c_2)$ the summation term in Eq. 41. These two terms are the driving force for c_1 and c_2, respectively. We now discuss the dynamics of the two images. For simplicity, assume that $\mathbf{x^1}$ and $\mathbf{x^2}$ have no overlapping nonzero components. An example is shown in Fig. 30.

It is seen that x_i^1 can be nonzero only when $x_i^2 = 0$, and vice versa. In this case, the driving forces can be written as

$$h_1(c_1, c_2) = \sum_{x_i^1 \neq 0}^{N}(x_i^1 - a_1)g(c_1x_i^1) - a_1\sum_{x_i^2 \neq 0} g(c_2x_i^2) \tag{42}$$

$$h_2(c_1, c_2) = \sum_{x_i^2 \neq 0}^{N}(x_i^2 - a_2)g(c_2x_i^2) - a_2\sum_{x_i^1 \neq 0} g(c_1x_i^1) \tag{43}$$

There are two terms in each of the driving forces. Consider $h_1(c_1, c_2)$. The first term comes from the correlation between the neuron state $g(c_1\mathbf{x^1})$ and the stored image $(\mathbf{x^1} - a_1)$, and the second term results from the coupling between c_1 and c_2 through the dc level a_1. Since a_1 and the gain function $g(x)$ are always positive, the second term gives a negative contribution to the driving force. This means that the coupling pulls the system away

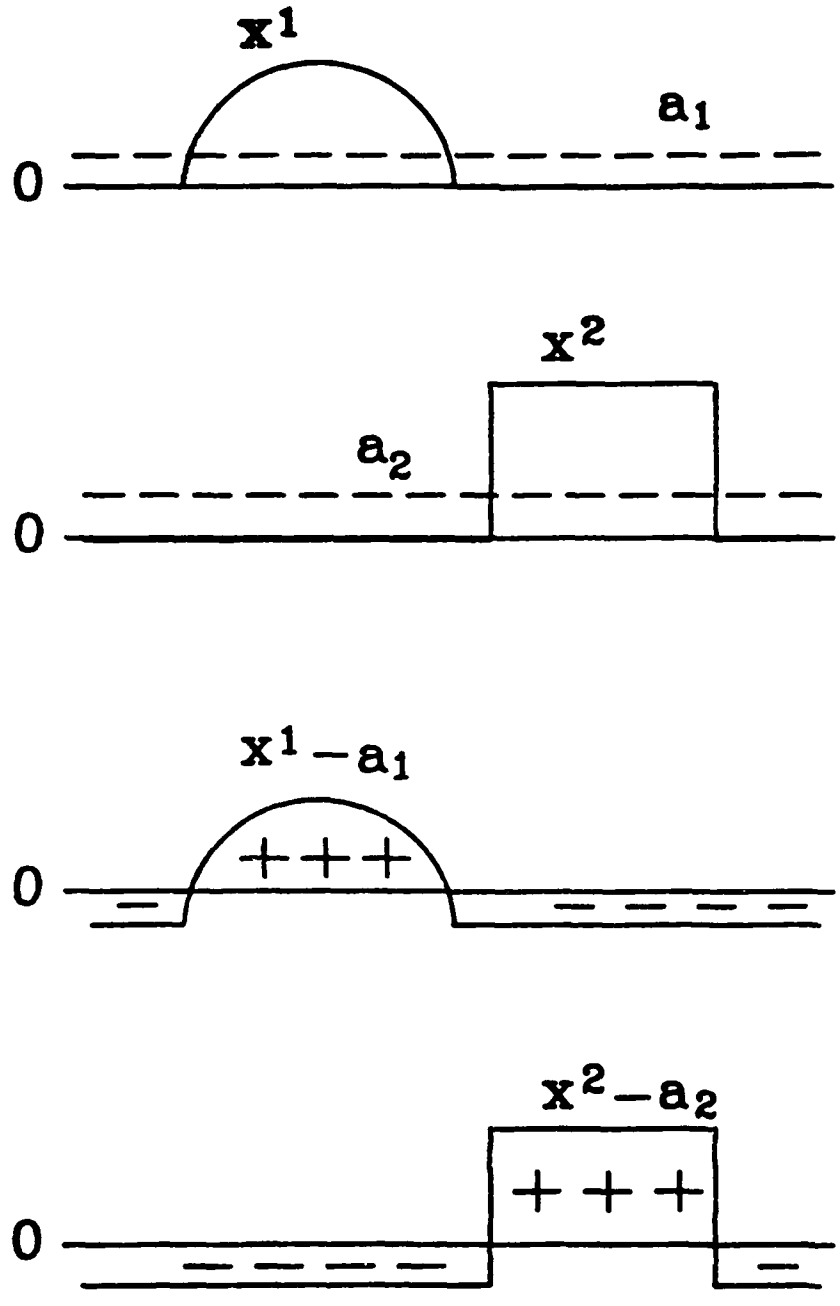

Fig. 30: An example of two stored images without overlaps.

from $\mathbf{x}^1$. The same description also applies to c_2. We plot $h_1(c_1, c_2)$ against c_1 for $c_2 = 0$ and $c_2 \neq 0$ in Fig. 31(a).

In the figure, the solid curve represents the case where $c_2 = 0$, and the dashed curve represents the case for $c_2 \neq 0$. We also plot the line $h(c_1) = c_1$ in the same figure. It is seen that there are three intersections, **P**, **Q**, and **R**, between the straight line and the solid curve. The plane is divided into four regions. In regions 1 and 3, c_1 is smaller than $h_1(c_1, c_2)$ and $\frac{dc_1}{dt} > 0$. Thus, in these regions the system state evolves in the direction of increasing c_1. This is represented by the arrow pointing to the right in the figure. On the other hand, in regions 2 and 4, $\frac{dc_1}{dt} < 0$; thus, the system evolves toward decreasing c_1. It can be seen that the points **P** and **R** are stable points, and **Q** is a saddle point. Now suppose we increase c_2. Then $g(c_2 x_i^2)$ increases, and $h_1(c_1, c_2)$ decreases. It can be seen from Fig. 31(a) that points **Q** and **R** move towards each other. The two points merge into one point at large values of c_2. On the other hand, the point **P** moves downward as c_2 increases. If we plot the trajectories of **P**, **Q**, and **R** for the coefficient c_1 in the (c_1, c_2) plane, we obtain Fig. 31(b). Since the gain function $g(x)$ is positive and symmetric with respect to x, the trajectories are symmetric with respect to the c_2 axis. The above argument shows how the dynamical behavior of the system can be understood using a geometrical method.

By going through the same procedure, we can also obtain the trajectories leading to the equilibrium points of c_2. We plot the two groups of trajectories in the same (c_1, c_2) plane. Fig. 32 shows the result. We see that there are 7 equilibrium points: one source, three sinks, and three saddles. The three sinks represent the null state (no image) and the two stored images. Point 1 represents the stable state corresponding to stored image $\mathbf{x}^1$, since at that position c_1 is large and c_2 is small. On the other hand, at point 2 c_1 is small and c_2 is large. This represents the stable state corresponding to stored image $\mathbf{x_2}$. It can be seen from the figure that if we start from an initial state, which is close to one of the stored states, then the system will converge to that state. Otherwise, it will decay to zero.

From the geometrical diagram we see that the stable state is always a mixed state of the stored memories. The extent of mixture can be reduced by reducing the neural gain. However, if the gain is too small, then the system will not be able to sustain the stored memories. As shown in Fig. 33(a), when the gain is very low, there is only one intersection point **O** between the line $h(c) = c$ and the curve of the driving force. The corresponding trajectories leading to **O** are drawn in Fig. 33(b). It is seen that the only equilibrium state is the null state at **P**. No matter where the initial state is, the system always decays to zero.

On the other hand, suppose the neural gain is very high. The trajectories to **P**, **Q**, and **R** are shown in Fig. 34.

We see that there are two more equilibrium points than the case shown in Fig. 32: a stable point m and a saddle point s. The state m is a strongly mixed state of $\mathbf{x}^1$ and $\mathbf{x}^2$. We also see that m has a large region of attraction. Thus, we can not set too high a gain.

Next consider the case where the stored memories have some slight overlap. The shape and position of the trajectory lines will be altered somewhat. Since the neural function is continuous, so is the driving force. Thus, the general features of the system will be the same. However, as the overlapping between the stored states increases more and more,

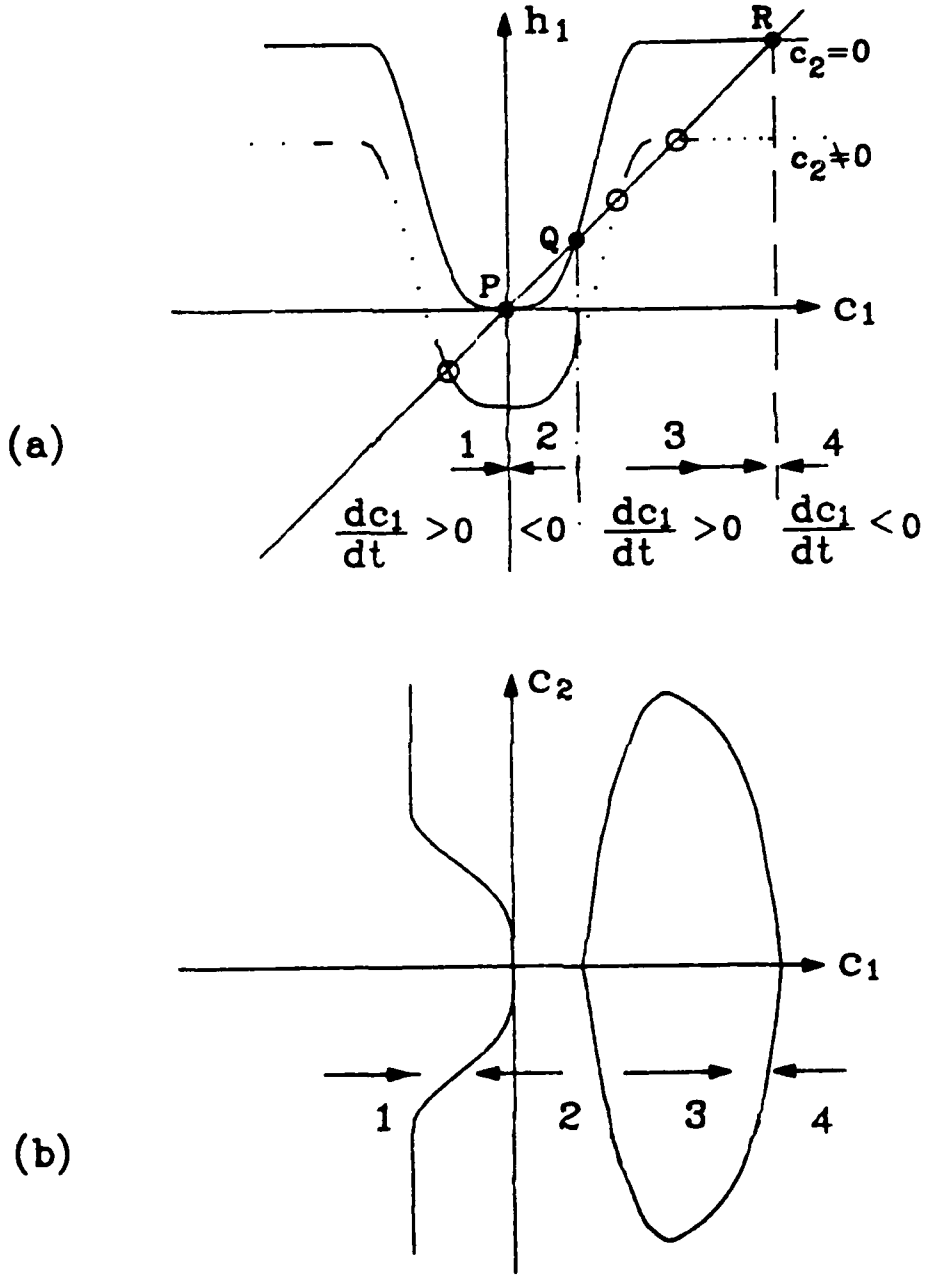

Fig. 31: The Driving Force and the Dynamics of the Loop. (a) The driving force for the first stored image. (b) The trajectories of the equilibrium states of the first image.

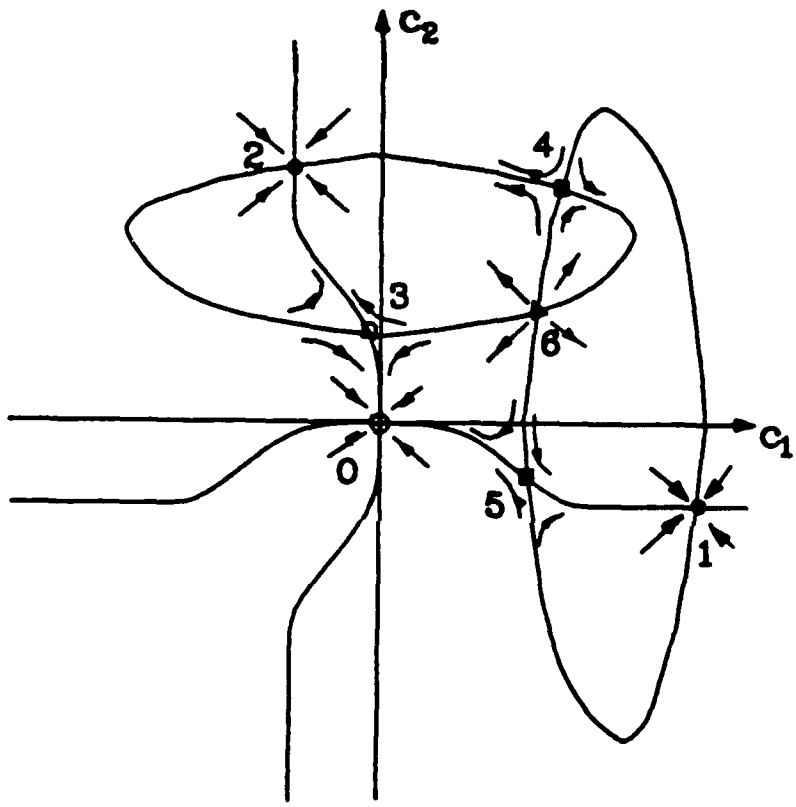

Fig. 32: The phase flow of the two-image auto-associative memory. States O, 1, 2 are stable. States 3, 4, 5 are unstable (saddle points). State 6: Source state. (unstable)

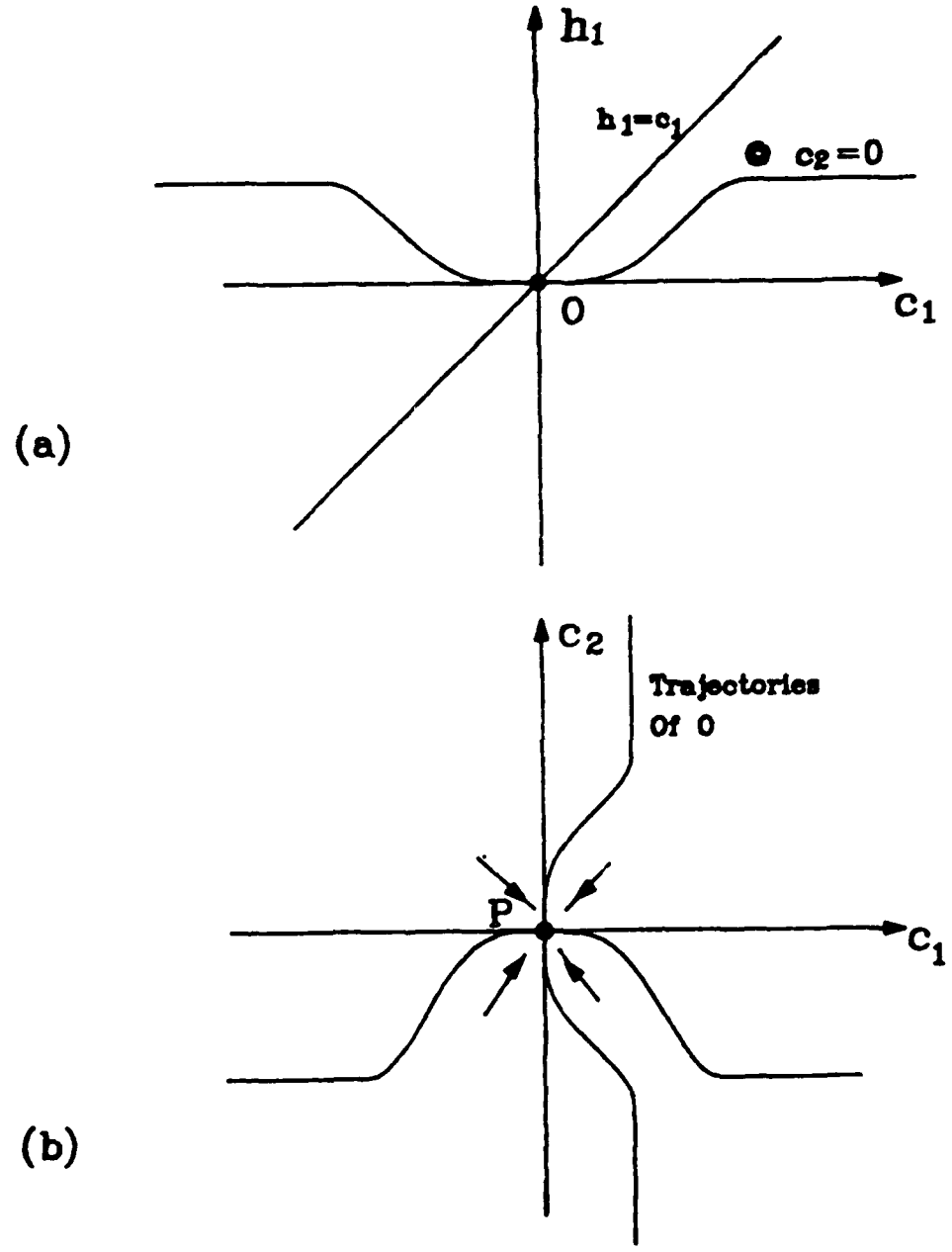

Fig. 33: The Dynamics of the Loop at Low Gain. (a) The driving force for the first stored image. (b) Trajectories for the equilibrium points. Point P is the only stable state.

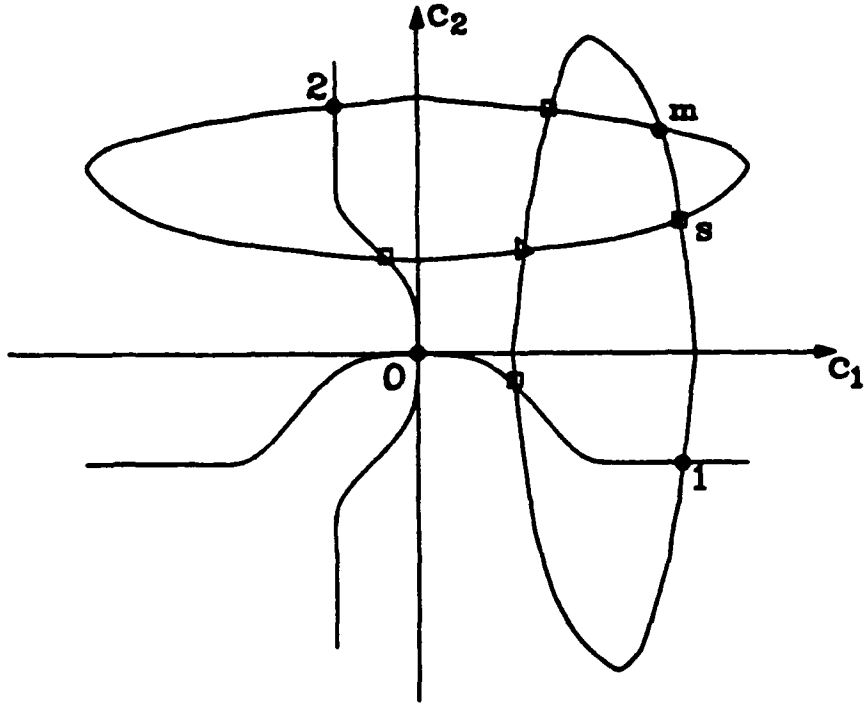

Fig. 34: The Dynamics of the Loop at High Gain. Two new equilibrium states are generated: m is mixed and s is unstable state.

the trajectories of the equilibrium points will be more and more distorted. As a result, the stable points that give the stored memory states will have more "mixing" with the other stored state. Thus, we would not expect the system to work well in the case of strong overlapping.

We can now investigate the dynamics of the system for the all-pass hologram in the memory loop. If we do not make the dc-level subtraction in storing the memories, then Equations 40 and 41 become

$$\frac{dc_1}{dt} = -c_1 + \sum_{i=1}^{N} x_i^1 g(c_1 x_i^1 + c_2 x_i^2) \tag{44}$$

$$\frac{dc_2}{dt} = -c_2 + \sum_{i=1}^{N} x_i^2 g(c_1 x_i^1 + c_2 x_i^2). \tag{45}$$

By going through similar arguments, we can draw the trajectories leading to the equilibrium points of the system. Fig. 35 shows one example.

It is seen that there are four stable states: two memory states, m_1 and m_2, one null state , and one mixed state **P**. If we decrease the neural gain, then the points m_1, m_2, **Q**, and **R** may disappear. However, the mixed state **P** always exists. Therefore, the high-pass hologram is crucial for good performance of the memory loop.

7 Conclusion

In this report we have successfully implemented an optical loop of the Hopfield-type neural network. The loop consists of a single layer of neurons with feedback. The 2-D array of neurons are simulated by an LCLV. The interconnections between the neurons are implemented by using planar holograms.

Experimental results show that the loop performs the function of auto-association which recognizes 2-D images from a distorted input. The distortions may come from rotating, scaling, shifting, partial blocking, or erroneous input. As long as the input provides enough information, the loop always converges to a stable state corresponding to the correct stored image. The similarity between the input and the stored images determines how fast the loop converges.

The gain function is another factor that determines the dynamics of the loop. Too low gain cannot sustain a stable memory. High gain provides more tolerance to the system to recognize a distorted image. However, too high gain also induces mixed states such that the loop makes incorrect recognitions. The trade-off between distortion tolerance and discrimination capability is set by the gain function, and the value of the optimum gain depends on the specific images stored.

We have presented a neural network model for the optical loop. Dynamic equations for the network are formulated. Since the optical neurons respond to light intensities, the input vs. output relationship of the neurons is not a simple sigmoid function. Rather, it is a sigmoid function symmetrical for positive and negative inputs. Thus, the slope of the neuron function is not always positive, and the conventional proof of convergence does not apply here. Although we have not found an energy function for our loop, we have presented a geometrical method for inspecting dynamic behaviors of the loop. The flow of

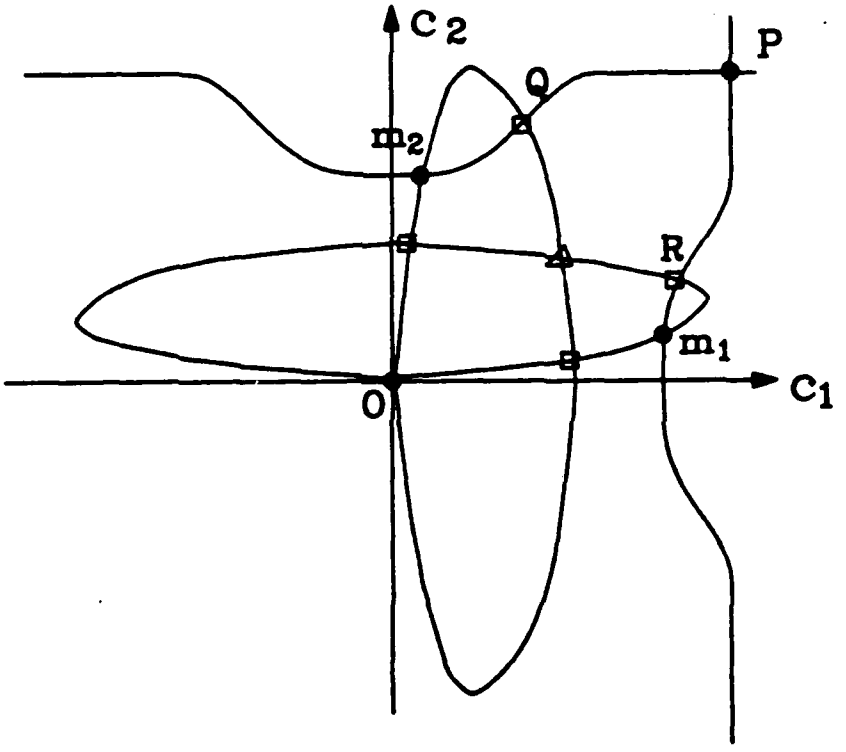

Fig. 35: The Dynamics of the Loop without the High Pass Hologram. There are four stable states: m_1, m_2 are stored states, O is null state. P is mixed state. Other states are unstable.

the state in the phase diagram helps us visualize the convergence properties of the loop. The diagram shows that the stable state is always a mixed state of the stored images, the degree of mixture depending on the gain function.

Appendix

Dynamic Equations for the Optical Associative memory

This appendix will focus on the derivation of the dynamic equations for the optical associative memory loop described in this report. The schematic diagram of the optical loop is shown in Fig. 5. The main idea is that corresponding to the set of stored images, we can construct a vector space $\mathbf{R^N}$, where N is the number of neurons of the system. Then the N-coupled dynamic equations of the neurons can be expressed in terms of the basis coefficients in $\mathbf{R^N}$. This transformation simplifies the form of dynamic equations so that the dynamic properties of the system can be inspected using a geometrical method.

A. Vector Space $\mathbf{R^N}$ and the Basis

We assume that the stored images $\mathbf{x^1}, \mathbf{x^2}, \ldots, \mathbf{x^M}$ are linearly independent. We then decompose the vector space $\mathbf{R^N}$ into two subspaces $\mathbf{V_1}$ and $\mathbf{V_2}$, where $\mathbf{V_1}$ is the vector space spanned by the stored images and $\mathbf{V_2}$ is normal to $\mathbf{V_1}$; i.e.,

$$\mathbf{R^N} = \mathbf{V}_1 \oplus \mathbf{V}_2, \tag{46}$$

$$\mathbf{V_1} = span\{\mathbf{x^1}, \mathbf{x^2}, \ldots, \mathbf{x^M}\}, \tag{47}$$

$$\mathbf{V_2} = \{\mathbf{y} | \mathbf{x} \cdot \mathbf{y} = 0, \forall \mathbf{x} \in \mathbf{V_1}\}, \tag{48}$$

where $\oplus$ is the direct sum of vector spaces. We now define a reciprocal basis $\beta_1 = \{\mathbf{y^1}, \mathbf{y^2}, \ldots, \mathbf{y^M}\}$ for $\mathbf{V}_1$, such that

$$\mathbf{y^i} \cdot \mathbf{x^j} = \delta_{ij} \qquad i, j = 1, \ldots, M. \tag{49}$$

Next we select an orthonormal basis $\beta_2 = \{\mathbf{y^{M+1}}, \ldots, \mathbf{y^N}\}$ for $\mathbf{V_2}$. We then have

$$\begin{aligned} \beta &= \beta_1 \cup \beta_2 \\ &= \{\mathbf{y^1}, \cdots, \mathbf{y^N}\} \end{aligned} \tag{50}$$

which forms a basis for $\mathbf{R^N}$. Thus, any image in $\mathbf{R^N}$ can be expressed in terms of the basis β:

$$\mathbf{x} = \sum_{k=1}^{N} c_k \mathbf{y^k}. \tag{51}$$

B. Dynamic Equations for the Optical Loop

It was shown in Section 6 that the dynamic equation for the neurons in the optical loop is

$$\frac{dx_i}{dt} = -x_i + g\left(\sum_{j=1}^{N} w_{ij} x_j\right), \qquad i = 1 \ldots N \tag{52}$$

where w_{ij} is the high-pass version of the interconnection strength given by Eq. 24. By Eq. 24 and 25, we have

$$\begin{aligned}\sum_{j=1}^{N} w_{ij}x_j &= \sum_{j=1}^{N}\Big(\sum_{m=1}^{M}(x_j^m - a_m)x_i^m\Big)x_j \\ &= \sum_{j=1}^{N}\Big(\sum_{m=1}^{M} x_i^m x_j^m\Big)x_j - \sum_{m=1}^{M}\sum_{j=1}^{N} a_m x_i^m x_j \\ &= \sum_{j=1}^{N}\Big(\sum_{m=1}^{M} x_i^m x_j^m\Big)x_j - \Big(\sum_{k=1}^{N} x_k\Big)\Big(\sum_{m=1}^{M}\sum_{j=1}^{N}\frac{1}{N}x_j^m x_i^m\Big) \\ &= \sum_{j=1}^{N}\Big(\sum_{m=1}^{M} x_i^m x_j^m\Big)\Big(x_j - \frac{1}{N}\sum_{k=1}^{N} x_k\Big). \end{aligned} \tag{53}$$

Note that $\left(x_j - \frac{1}{N}\sum_{k=1}^{N} x_k\right)$ is the j^{th} component of the vector $\left(\mathbf{x} - \frac{1}{N}\sum_{k=1}^{N} x_k\right)$. Since $\left(\mathbf{x} - \frac{1}{N}\sum_{k=1}^{N} x_k\right)$ is also a vector in $\mathbf{R^N}$ and any vector in $\mathbf{R^N}$ can be expanded in the basis β, we let

$$\left(\mathbf{x} - \frac{1}{N}\sum_{k=1}^{N} x_k\right) = \sum_{k=1}^{N} c_k \mathbf{y^k}. \tag{54}$$

The feedback signal in the loop then becomes

$$\begin{aligned}\sum_{j=1}^{N} w_{ij}x_j &= \sum_{j=1}^{N}\Big(\sum_{m=1}^{M} x_i^m x_j^m\Big)\Big(\sum_{k=1}^{N} c_k y_j^k\Big) \\ &= \sum_{m=1}^{M}\sum_{k=1}^{N}\Big(\sum_{j=1}^{N} x_j^m y_j^k\Big)c_k x_i^m \\ &= \sum_{m=1}^{M}\Big(\sum_{k=1}^{N}(\mathbf{x^m}\cdot\mathbf{y^k})c_k\Big)x_i^m. \end{aligned} \tag{55}$$

By applying the orthnormal property of the reciprocal vectors $\mathbf{x^m}$ and $\mathbf{y^m}$ in the above equation, we obtain

$$\sum_{j=1}^{N} w_{ij}x_j = \sum_{m=1}^{M} c_m x_i^m. \tag{56}$$

The dynamic equation then becomes

$$\frac{dx_i}{dt} = -x_i + g\Big(\sum_{m=1}^{M} c_m x_i^m\Big) \qquad i = 1 \ldots N. \tag{57}$$

Note that c_m is the projection of the high-pass version of the input on the stored vector $\mathbf{x^m}$. It is seen that the system dynamics is specified by the M coefficients of the reciprocal vectors of the stored images. In what follows we will derive the equation of motion for these coefficients.

Multiplying both sides of Eq. 57 by $1/N$ and summing over i, we get

$$\frac{1}{N}\sum_{i=1}^{N}\frac{dx_i}{dt} = -\frac{1}{N}\sum_{i=1}^{N}x_i + \frac{1}{N}\sum_{i=1}^{N}g\Big(\sum_{m=1}^{M}c_m x_i^m\Big) \qquad i = 1\ldots N. \tag{58}$$

Subtracting Eq. 58 from Eq. 57 gives

$$\frac{d}{dt}\Big[x_i - \frac{1}{N}\sum_{j=1}^{N}x_j\Big] = -\Big[x_i - \frac{1}{N}\sum_{j=1}^{N}x_j\Big] + g\Big(\sum_{m=1}^{M}c_m x_i^m\Big) - \frac{1}{N}\sum_{i=1}^{N}g\Big(\sum_{m=1}^{M}c_m x_i^m\Big). \tag{59}$$

Note that the terms in the bracket can expanded in the basis β; thus, the equation of motion is given in terms of the β coefficients as

$$\sum_{k=1}^{N}\frac{dc_k}{dt}y_i^k = -\sum_{k=1}^{N}c_k y_i^k + g\Big(\sum_{m=1}^{M}c_m x_i^m\Big) - \frac{1}{N}\sum_{i=1}^{N}g\Big(\sum_{m=1}^{M}c_m x_i^m\Big). \tag{60}$$

Multiplying both sides of the above equation by x_i^l and then summing over i gives

$$\begin{aligned}\sum_{k=1}^{N}\frac{dc_k}{dt}(\mathbf{x}^l\cdot\mathbf{y}^l) = &-\sum_{k=1}^{N}c_k(\mathbf{x}^l\cdot\mathbf{y}^l) + \sum_{i=1}^{N}x_i^l g\Big(\sum_{m=1}^{M}c_m x_i^m\Big),\\ &-\Big(\frac{1}{N}\sum_{i=1}^{N}x_i^l\Big)\sum_{i=1}^{N}g\Big(\sum_{m=1}^{M}c_m x_i^m\Big)\end{aligned} \tag{61}$$

Applying the orthonormal relation between the stored images and the reciprocal basis, we obtain

$$\frac{dc_l}{dt} = -c_l + \sum_{i=1}^{N}(x_i^l - a_l)g\Big(\sum_{m=1}^{M}c_m x_i^m\Big) \qquad l = 1,\ldots,M. \tag{62}$$

Recall that a_l is the average level of the stored image $\mathbf{x}^l$. Similarly, the equation of motion for $c_{M+1},\cdots,c_N$ can be obtained by multiplying both sides of Eq. 60 by y_i^l, and summing over i. We get

$$\frac{dc_l}{dt} = -c_l + \sum_{i=1}^{N}(x_i^l - b_l)g\Big(\sum_{m=1}^{M}c_m x_i^m\Big) \qquad l = M+1,\ldots,N, \tag{63}$$

where b_l is defined as

$$b_l = \frac{1}{N}\sum_{i=1}^{N}y_i^l. \tag{64}$$

The dynamic behavior of the optical loop is thus completely determined by Equ.s 63 and 64. Instead of solving these equations, we have presented a geometrical method in Equ.stion 6 for investigating the convergence properties of the loop and the important parameters that affect the dynamics.

References

[1] J. J. Hopfield, "Neural Networks and Physical Systems with Emergent Collective Computational Abilities," *Proc. Natl. Acad. Sci. USA*, Vol. **79** , pp.2554-2558, April (1982).

[2] J. J. Hopfield, "Neurons with Graded Response Have Collective Computational Properties Like Those of Two-State Neurons," *Proc. Natl. Acad. Sci. USA*, Vol. **81**, pp. 3088-3092, May (1984).

[3] Y. S. Abu-Mostafa and D. Psaltis, "Optical Neural Computers," Scientific American, Vol. **256**, No. 3, pp. 88-95, March (1987).

[4] J. H. Kim, S. H. Lin, J. Katz, and D. Psaltis, "Monolithically Integrated Two-Dimensional Arrays of Optoelectronic Threshold Devices for Neural Network Applications," *SPIE Symposium on Lasers & Optics*, Paper 1043-07, Los Angeles, California, 15-20 Jan. (1989).

[5] L. S. Lee, H. M. Stoll, and M. C. Tackitt, "Continuous-time Optical Neural Associative Memory," *Opt. Lett.* **14**, 162 (1989).

[6] S. Venkatesh and D. Psaltis, "Linear and Logarithmic Capacities in Associative Neural Networks," submitted for publication in *IEEE Trans. Inform. Theory.*

[7] R. J. McEliece, E. C. Posner, E. R. Rodemich, and S. Venkatesh, "The Capacity of the Hopfield Associative Memory," *IEEE Trans. Inform. Theory*, Vol. **IT-33**, No. 4, 461-482, July (1987).

[8] D. Psaltis and N. Farhat, "Optical Information Processing Based on an Associative -Memory Model of Neural Nets with Thresholding and Feedback," *Opt. Lett.* **10**, 98 (1985).

[9] N. H. Farhat, D. Psaltis, A. Prata, and E. Paek, "Optical Implementation of the Hopfield Model," *Appl. Opt.*, **24**, 1469-1475, (1985).

[10] D. Psaltis, E. Paek, and J. Hong, "Acousto-Optic Implementation of the Hopfield Model," *JOSA*, **2**, No. 13, 48, December (1985).

[11] J. S. Jang, S. W. Jung, S. Y. Lee, and S. Y. Shin, "Optical Implementation of the Hopfield Model for Two-Dimensional Associative Memory," *Opt. Lett.* **13**, 248 (1988).

[12] J. S. Jang, S. Y. Shin, and S. Y. Lee, "Optical Implementation of Quadratic Associative Memory with Outer-Product Storage," *Opt. Lett.* **13**, 693 (1988).

[13] E. G. Paek and D. Psaltis, "Optical Associative Memory using Fourier Transform Holograms," **26**, No. 5, 428-433, May (1987).

[14] A. B. Vander Lugt, "Signal Detection by Complex Spatial Filtering," *IEEE Trans. Inform. Theory*, **IT-10**, No. 2, 139-145, (1964).

[15] Y. Owechko, G. J. Dunning, E. Marom, and B. H. Soffer,"Holographic Associative Memory with Nonlinearities in the Correlation Domain," *Appl. Opt.*, **26**,(10), 1900-1910, May (1987).

[16] D. Z. Anderson, "Coherent Optical Eigenstate Memory," *Opt. Lett.*, **11**, 56 (1986).

[17] A. Yariv, S. K. Kwong, and K. Kyuma, "Optical Associative Memories based on Photorefractive Oscillations," *Proc. Soc. Photo-Opt. Instrum. Eng.*, **613**, 1 (1986).

[18] D. Psaltis and J. Hong, "Shift-Invariant Optical Associative Memories," *Opt. Eng.*, **26**, 10-15, January (1987).

[19] G. J. Dunning, E. Maron, Y. Owechko, and B. H. Soffer, "All-Optical Associative Memory with Shift Invariance and Multiple-Image Recall," *Opt. Lett.* **12**, 346 (1987).
[20] H. Y. Li, "Analysis of Pinhole Array Associative Memory System Using the Method of Phase Planes," private communication.